NASA/TM—2003-212553

A Treatment of Measurements of Heptane Droplet Combustion Aboard MSL–1

M.D. Ackerman
University of California, San Diego, La Jolla, California

R.O. Colantonio
Glenn Research Center, Cleveland, Ohio

R.K. Crouch
Headquarters, Washington, DC

F.L. Dryer
Princeton University, Princeton, New Jersey

J.B. Haggard
Glenn Research Center, Cleveland, Ohio

G.T. Linteris
National Institute of Standards and Technology, Gaithersburg, Maryland

A.J. Marchese
Princeton University, Princeton, New Jersey

V. Nayagam
National Center for Microgravity Research, Cleveland, Ohio

J.E. Voss
Johnson Space Center, Houston, Texas

F.A. Williams and B.L. Zhang
University of California, San Diego, La Jolla, California

October 2003

The NASA STI Program Office . . . in Profile

Since its founding, NASA has been dedicated to the advancement of aeronautics and space science. The NASA Scientific and Technical Information (STI) Program Office plays a key part in helping NASA maintain this important role.

The NASA STI Program Office is operated by Langley Research Center, the Lead Center for NASA's scientific and technical information. The NASA STI Program Office provides access to the NASA STI Database, the largest collection of aeronautical and space science STI in the world. The Program Office is also NASA's institutional mechanism for disseminating the results of its research and development activities. These results are published by NASA in the NASA STI Report Series, which includes the following report types:

- TECHNICAL PUBLICATION. Reports of completed research or a major significant phase of research that present the results of NASA programs and include extensive data or theoretical analysis. Includes compilations of significant scientific and technical data and information deemed to be of continuing reference value. NASA's counterpart of peer-reviewed formal professional papers but has less stringent limitations on manuscript length and extent of graphic presentations.

- TECHNICAL MEMORANDUM. Scientific and technical findings that are preliminary or of specialized interest, e.g., quick release reports, working papers, and bibliographies that contain minimal annotation. Does not contain extensive analysis.

- CONTRACTOR REPORT. Scientific and technical findings by NASA-sponsored contractors and grantees.

- CONFERENCE PUBLICATION. Collected papers from scientific and technical conferences, symposia, seminars, or other meetings sponsored or cosponsored by NASA.

- SPECIAL PUBLICATION. Scientific, technical, or historical information from NASA programs, projects, and missions, often concerned with subjects having substantial public interest.

- TECHNICAL TRANSLATION. English-language translations of foreign scientific and technical material pertinent to NASA's mission.

Specialized services that complement the STI Program Office's diverse offerings include creating custom thesauri, building customized databases, organizing and publishing research results . . . even providing videos.

For more information about the NASA STI Program Office, see the following:

- Access the NASA STI Program Home Page at ***http://www.sti.nasa.gov***

- E-mail your question via the Internet to help@sti.nasa.gov

- Fax your question to the NASA Access Help Desk at 301–621–0134

- Telephone the NASA Access Help Desk at 301–621–0390

- Write to:
  NASA Access Help Desk
  NASA Center for AeroSpace Information
  7121 Standard Drive
  Hanover, MD 21076

NASA/TM—2003-212553

A Treatment of Measurements of Heptane Droplet Combustion Aboard MSL–1

M.D. Ackerman
University of California, San Diego, La Jolla, California

R.O. Colantonio
Glenn Research Center, Cleveland, Ohio

R.K. Crouch
Headquarters, Washington, DC

F.L. Dryer
Princeton University, Princeton, New Jersey

J.B. Haggard
Glenn Research Center, Cleveland, Ohio

G.T. Linteris
National Institute of Standards and Technology, Gaithersburg, Maryland

A.J. Marchese
Princeton University, Princeton, New Jersey

V. Nayagam
National Center for Microgravity Research, Cleveland, Ohio

J.E. Voss
Johnson Space Center, Houston, Texas

F.A. Williams and B.L. Zhang
University of California, San Diego, La Jolla, California

National Aeronautics and
Space Administration

Glenn Research Center

October 2003

Acknowledgments

We wish to thank Merrill King and Howard Ross for helpful discussions during data acquisition.
This work was supported by the NASA Microgravity Combustion Science Program.

Available from

NASA Center for Aerospace Information
7121 Standard Drive
Hanover, MD 21076

National Technical Information Service
5285 Port Royal Road
Springfield, VA 22100

Available electronically at http://gltrs.grc.nasa.gov

Introduction

A droplet combustion experiment (DCE) was designed and run onboard the MSL-1 mission of the Space Shuttle Columbia. There were two flights of this mission—STS-83 in April of 1997 and STS-94 in July of 1997. The reflight occurred because a fuel-cell power problem onboard the shuttle forced an early termination of the first flight; this was the only shuttle mission to be flown twice. DCE data were obtained during both flights, as summarized in Table 1. The STS-83 data have been reported and analyzed previously,[1] but the STS-94 data have not yet been presented. The purpose of this report is to help to make available a complete set of data from both flights in a uniform format in order to facilitate further analysis of the results. The figures and initial text in this report were prepared by M. Ackerman; the authorship reflects the composition of the MSL-1 team involved in droplet combustion.

A fiber-supported droplet combustion (FSDC) experiment also was run on STS-94. This smaller "glovebox" experiment, which investigated the combustion of fiber-supported droplets (also called tethered droplets) in Spacelab cabin air, had previously flown on the first United States Microgravity Laboratory (USML-1) mission of STS-73, but successful measurements with heptane as the fuel in this experiment were first obtained on STS-94. The FSDC data for heptane also are analyzed and reported here, for comparison with the DCE results. A number of other fuels were also burned in the FSDC experiments on STS-94, but data for those fuels are not given here since the present focus is strictly on heptane droplet combustion; heptane droplet combustion in convective flow also was studied, but similarly, only data without forced convection are considered here, since the investigation of convection effects was not an objective of DCE, which was intended to concentrate on the combustion of quiescent droplets in quiescent atmospheres.

The DCE experimental apparatus and procedures were described in a previous paper,[1] and some analysis of the data has been published.[2] The reader is referred to these earlier publications for the necessary background and details. Only brief descriptions of the experimental approach and data collection are given here. The main focus is on presenting the results of the measurements and drawing some conclusions from them. Studies will be made of the changes in the burning rate and flame behavior as the initial droplet diameter and the environment are altered, and extinction phenomena will be examined in more detail.

Experimental Approach and Data Collection

Familiarity with the DCE experiments may be obtained by consulting the diagrams of the experimental apparatus that have been given previously.[1] To begin a series of experiments, the test chamber was first vented to the space vacuum then filled from one of the premixed gas bottles that had been prepared prior to flight. Each bottle had been selected to establish the desired pressure and oxygen concentration in the test chamber after it was connected to the evacuated chamber and its valve was opened. All of the gas bottles contained helium-oxygen mixtures; for one set of tests the cabin air was used instead of a gas bottle. Since several burns were performed in the environment generated by each gas bottle, the post-combustion gas was sampled prior to venting so that the composition could be examined after return to earth. These examinations verified that changes in the atmospheres could be neglected in interpreting results.

Once the environment was established, fuel was injected through two opposed needles. The needles were slightly retracted during injection to form a liquid bridge. After the desired droplet size had been reached, the needles were moved farther apart to stretch the droplet. This stretching helped to achieve a more symmetric deployment and less drift of the droplet after deployment. Finally, the needles were rapidly extracted from the droplet and from the field of view. The extraction caused a small amount of liquid-droplet oscillation, which was observed to dampen viscously, generally in well under one second.

Just after the needles were extracted, hot-wire igniters were energized electrically to activate combustion. These wires were already in place, having been initially positioned with the needles. After ignition the igniters were withdrawn slowly to minimize the gas flow associated with their motion. The igniters were initially visible to the cameras that provided both the droplet and flame views of combustion, and in one test, number 18 in Table 1, the droplet struck the igniter. A series of photographs of a typical burn can be found in the earlier paper.[1]

The apparatus included three cameras and a viewport that allowed the experimenter to take still 35 mm photographs. Two of the cameras were dedicated to data acquisition. The first was a 35 mm black-and-white, high-speed motion-picture camera that took magnified, backlit views of the droplet. The second was an ultraviolet-sensitive intensified-array camera equipped with a narrow-band interference filter at 310 μm (one of the bands of OH emission associated with combustion) for flame imaging. The third camera was a color camcorder positioned to provide a general view of the combustion process and not considered part of the data-acquisition system, although it did prove helpful for checking some data. Images from the camcorder and from the ultraviolet camera were downlinked to the experimenters on the ground and used to evaluate whether ignition had been successful and the character of the burning and extinction, to determine what further tests needed to be done. In addition to the photographs, the temperature and pressure of the combustion chamber were measured, recorded and downlinked.

A PC-based image-analysis system[3] was used to measure droplet and flame diameters as functions of time. Rectangular areas of interest (AOI's) were defined by positioning boundaries just overlapping the top, bottom, left and right edges of the droplet and flame; within each AOI, a change in intensity was used to determine the edge location. The "threshold tracking" option of the program,[3] which sets the image to only black and white after defining a threshold and then uses the computer to automatically find the white pixel farthest toward the selected edge (top, bottom, left, or right) of the AOI, was used for most tests.

The interference arising from soot-particle images, from the droplet or flame nearing the edge of the field of view or from dim flames necessitated manual tracking of parts of some tests. During manual tracking, the same procedures were followed as in threshold tracking, but the computer operator selected the location of the AOI and the droplet or flame boundary. The image was magnified to aid in determining the edge location. This magnification uniformly increased the size of all the pixels in the image so that the relative scaling was unaltered, yielding the correct number of pixels per millimeter.

To clarify the images and make the boundary more distinct, several filters and processes were used. For the flame images, an edge-detecting filtering operation was employed; this operation involved performing a convolution with a Sobel edge-detect filter. Further description of this filter can be found in the NASA technical paper describing the image-analysis software.[3] The edge-detect filter was not needed for the droplet images because their edges where sharper. To identify the boundary of the droplet, an AOI was assigned to encompass the entire droplet. A low-pass filter was then applied to this AOI, followed by a morphological erosion and reconstruction of the droplet edge, to help eliminate soot-particle images from the AOI. Again, more details on the filter and morphological processes can be found in the paper describing the image-analysis software.[3] Following the image processing the entire area of the droplet was recorded to determine the movement of the droplet center and to calculate a third droplet diameter, in addition to the two diameters measured in orthogonal directions. Area data were not recorded from the flame images which appear as rings because determining the center movement or diameter from the areas of flame images requires multiple measurements; by contrast, the droplet images appear as filled circles, making diameter calculations simpler and more reliable. Additionally, less noise and more evenly circular flames made this third diameter measurement less important in the flame view.

The computer-generated results were checked with visual measurements of some frames to insure accuracy. Accuracy varied from test to test as a consequence of variations in the intensity of the lighting (affected by the flame intensity) and the amount of soot present. Slight errors from the image processing were also considered. Overall, the error (based on visual measurements) was estimated to be less than 5% of the initial droplet diameter in the droplet measurements and less then 2% of the first-measured flame diameter in the flame measurements.

Approach to Reporting of Results

Only about half of the tests that were performed provided data that can be used. Among the encountered difficulties that limited the amount of useful data acquired were failure to achieve deployment or ignition of the droplet, failure of one or both of the data-acquisition cameras and drift of the droplet out of the field of view of one or both of the cameras prior to completion of combustion. In the present work, an objective was to extract from the experiments all of the possibly useful data on droplet combustion contained in the recorded droplet-diameter and flame-diameter histories. To achieve this objective, all of the tests that met minimal criteria were analyzed; these criteria were, first, that the droplet was ignited, and, second, that the droplet or flame remained in the field of view of at least one of two data-acquisition cameras, either droplet-view or flame-view, for a minimum of 0.5 seconds, the approximate time required for initial transients to subside and a time short compared with burning times of droplets in the size range investigated. Flame views without droplet views and droplet views without flame views thus were accepted, although there were no instances in which the latter situation occurred for 0.5 seconds or more. A third imposed criteria was that if a test lacked a droplet view, then the flame had to stay in view until extinction. This third restriction excluded just two tests in which only flame views of slowly increasing diameter soon passed out of the field of view; it was felt that, since even the initial droplet diameters were uncertain in these tests, the data on the short flame-diameter histories would not be useful.

Table 1 summarizes the results of the tests that satisfied these three criteria, ordered from high to low pressures, from rich to lean atmospheres and from large to small initial droplet diameters. In addition to specifying the test conditions (chamber pressure and oxygen percentage), Table 1 reports the burning times, burning-rate constants and final flame and droplet diameters at extinction, when available. Also, Table 1 gives drift velocities obtained from flame-view and droplet-view cameras as the magnitude of the velocity of the center of the droplet or flame. These values are roughly indicative of the convective velocities of the droplets with respect to the gas but cannot be equated exactly to those convective velocities because of the absence of measurements of local gas velocities. Large convective velocities increase droplet burning rates. The values of the drift velocities are smaller than those found in most free-droplet combustion experiments, averaging about 3.4 mm/s and never exceeding 13 mm/s, except in test 18 in which the droplet rebounded from an igniter wire just after deployment, as noted previously.

Two approaches were taken in reducing the data on flame-diameter and droplet-diameter histories. In the first approach, the raw data extracted from the image-analysis system were exhibited graphically. To ease comparisons with the earlier paper that reported the STS-83 results and to minimize noise resulting from soot images, the graphs report a droplet diameter determined from measurements of the droplet area, assumed circular. The flame diameter reported in the graphs is the average of the two orthogonal measurements. The average was used to reduce noise levels arising from small flame irregularities in the flame views. The measurements typically differed from the reported values by less than 5% in the droplet data and by less then 2% in the flame data.

In the second approach, these data were smoothed using the second degree Loess smoother[4] in the statistical software package S-Plus. Because of the different behavior and different distributions of noise in the droplet and flame data, different spans were specified for each. The droplet data had little curvature, allowing a larger span to be used than for the flame data; however, noise differences between tests of long and short duration led to the use of different spans for different droplets. In the longer tests noise was primarily due to the computer interpreting a soot particle as the edge of the droplet, leading to measurements exceeding the actual diameter. A long span is then needed to prevent a bump from appearing in the data. As a result of the noise distribution and little curvature, a span of 75% of the data set was used for most of the droplet tests. Droplet data from tests of short duration had less noise, and most of the noise in these tests arose from droplet oscillation caused by deployment, which led to a more uniform distribution above and below the actual diameter. Because of the smaller amount of noise and the more uniform distribution, shorter spans were selected for these tests to even out this “chatter.”

While the flame data were less noisy overall than the droplet data, they also exhibited noise differences based on the duration of the tests. Unlike the droplet data, the flame data were noisier in the short tests, since most of the noise came from a very bright initial flame as accumulated vapor ignited, an occurrence which generally lasted less than a quarter of a second. Also, occasionally a very dim flame in the final 0.5-1 s generated noise. The flame data also had more curvature than the droplet data. For the longer flame data sets with less noise and higher curvature than the droplet tests, the span was set to only 25% of the data. Larger spans were used for a few of the shorter, noisier flame plots. These shorter tests also exhibited less curvature, allowing a larger span to be used without losing important features of the plot. Even after adjusting the span, the large initial noise and curvature of some tests made it impossible for the smoothing algorithm to smooth these areas accurately; consequently, the first 0.5 s of many droplet and flame graphs and the last 0.5 s of a few flame graphs were smoothed by eye.

The smoothed data were displayed graphically with estimated error bars indicating uncertainties. Although the error bars are large, purposely drawn so to include all possible errors, the estimated error is smaller, as indicated above. Figures 1 through 11 show this smoothed data obtained by the second approach, and Appendix A presents the raw data obtained by the first approach. In Figures 1 through 11 a "D" at the end of the trace is used to denote drift out of the field of view. A solid dot at the end of the flame trace shows a known point of extinction. Droplet traces were not marked at extinction because extinction is not visibly evident in that view.

All of the graphs in this paper start with zero as the time of ignition of the droplet, ignition being defined as the first visual evidence of the flame. The tests were synchronized using the GMT (Greenwich mean time) stamps in both views. The times agree, through the use of the GMT stamp, to within 0.1 second. All of the droplets show an increase in droplet diameter during ignition. This increase is due to thermal expansion during heat-up and ignition, as previously discussed;[1] to demonstrate this increase more fully, the data from deployment to ignition are shown as occurring at negative times in the graphs appearing in Appendix A, in all cases except those for which such data is unavailable because of the droplet's proximity to the igniter (tests 18, 21, and 22). It should be noted, however, that oscillations arising from deployment (and the method of determining the droplet diameter from the area, which at these earlier times is not always circular as assumed) cause noise that may mask the true nature of the early droplet behavior. As noted earlier,[1] this oscillation has usually been viscously damped prior to ignition of the droplet. Ignition was chosen as the zero point because it eases the comparison of flame data and burning rates (not all test have the same time span from deployment to ignition or even from hot-wire initiation to ignition). More information on the initial increase in droplet diameter and initial oscillation can be found in the earlier paper.[1] The initial diameters reported here differ slightly from those given earlier[1] because at the time of ignition the droplet often is slightly smaller than its maximum size recorded previously.[1] The present selection is consistent with the stated focus on combustion only.

The flame data were not recorded here for the first one to three frames at ignition (one frame is equivalent to 1/30th of a second in the flame view) because of the initial size, shape and brightness of the flame. The flame burnt excess accumulated vapors within the first tenth of a second and then settled down to the expected spherical, steady glowing state. The initial frames showed variable, often large and irregularly shaped flames.

Results at 1.00 Bar, 35% Oxygen

Results of three tests completed in this, the richest helium-oxygen environment at normal atmospheric pressure, are shown in Fig. 1. These tests were performed on STS-83 and have been thoroughly discussed previously.[1] The data in Table 1, Fig. 1, and Fig. A1 for these tests are included for completeness; they also serve to demonstrate results of different types of data analysis since the methods employed here differ somewhat from those used earlier.[1] The results obtained by the different methods are not significantly different.

All tests in this atmosphere show a classic rise then decrease in flame diameter, experiencing diffusive extinction at measurable flame diameters. Droplet diameters at extinction are too small to be measured, possibly zero. As previously discussed,[1] there is also some curvature in the plots of droplet diameter squared, the burning-rate constant decreasing with time during combustion, which is seen more clearly in Fig. A1 than in Fig. 1; Table 1 further quantifies variation in burning-rate constants by reporting, besides an average value derived from a least-squares fit of the overall droplet-diameter history, both an initial value obtained from the first part of the droplet-diameter history and a final value obtained from the last part before extinction. It may be seen that variations on the order of 50% occur in this atmosphere, even for the smallest droplet. Although the change may be due to absorption in the liquid, during burning, of less volatile materials produced by pyrolysis in the region between the droplet and the flame, the statement[1] is still valid that the "source of these [variations] remains a topic for further study." The results of the different kinds of data analysis reported here support the previous interpretations[1] and do not indicate any need for revision of the earlier discussion.

Results at 1.00 Bar, 32% Oxygen

The success in STS-83 offered the opportunity to change the gas composition slightly for the reflight, so that finer testing of the dependence of the combustion behavior on the oxygen concentration could be performed. For this reason, experiments in helium-oxygen environments at 1.00 bar with 32% oxygen mole fractions were carried out on STS-94. A motivation for decreasing the oxygen concentration was the finding[1] of radiative extinction at lower oxygen mole fractions; the experiments at 32% oxygen could narrow the uncertainty in the location of the boundary between diffusive and radiative extinction. Figure 2 shows the results obtained at this lower oxygen concentration.

The two smaller droplets in Figs. 2 and A2 behave very much like the droplet of similar size that was burned in 35% oxygen. The average burning rate is slightly less in 32% oxygen, and the flame diameter slightly larger, as is to be expected, but the qualitative behavior, including the existence and magnitude of curvature in the diameter-squared plots and the immeasurably small (possibly zero) droplet diameter at extinction, are the same. It is especially interesting, however, to compare the behavior of the largest droplet in Fig. 2 (test 4) with that of the largest droplet in Fig. 1 (test 1). Even though the initial droplet diameter in test 1 is slightly larger than that in test 4, the flame diameter is noticeably larger in test 4. This larger flame is due to the lower oxygen concentration for test 4. The flame in test 4 does not experience the strong soot-penetration event, seen in Fig. A1 as a sudden increase in flame diameter during test 1 and discussed previously.[1] The burning rate for test 4 is correspondingly lower than that for test 1, especially near the end of the data trace, causing the initially larger droplet of test 1 to eventually become smaller than the droplet of test 4 after both have burned for a sufficiently long time period (approximately 5 seconds). The differences in the flame diameters and burning rates of these two droplets, towards the end of the burn, clearly exceed experimental uncertainty. While the droplet in test 1 definitely experiences diffusive extinction, it is unclear whether the droplet in test 4 experiences diffusive or radiative extinction. Both the flame and the droplet in this test drift out of the field of view before a definitive judgment can be made. The radiative-diffusive boundary, at an initial droplet diameter of about 3.9 mm, therefore, may or may not extend beyond 32% oxygen; from Fig. 1 it is clear that it does not extend to 35% oxygen, and from Fig. 3 it will be seen that it definitely extends beyond 30% oxygen.

Results at 1.00 Bar, 30% Oxygen

Figure 3 shows results obtained from the five successful burns in this environment. The first two results, those from the two largest droplets, were obtained on STS-83 and have been discussed before.[1] The largest experiences radiative extinction, the droplet diameter being of appreciable size when flame extinction occurs and continuing to decrease in size through vaporization in the hot gas after flame

extinction. This vaporization process can continue for time periods on the order of 5 seconds, as results in other atmospheres will show. The smaller of these two droplets exhibits diffusive extinction. All three STS-94 tests in this atmosphere were for even smaller initial droplet diameters, and they all exhibited diffusive extinction, as would be expected.

The initial droplet diameters in the STS-94 tests were quite similar, and their diameter histories are not clearly distinguishable, even in the raw data of Fig. A3. Their flame diameters, however, are somewhat different, likely as a consequence of different amounts of initial fuel vaporization prior to ignition. The differences amount to about 20 to 30%, somewhat more than the difference between tests 1 and 4 noted earlier. As burning proceeds the differences in the three flame diameters are seen to decrease, indicating that the effects of the initial conditions diminish with time.

Curvature in the diameter-squared plots, like that found for the 35 and 32% oxygen, also is visible in this 30% data (see Fig. A3). This curvature is of a lesser extent than at the higher oxygen contents, as is evident by the entries in Table 1.

Results at 1.00 Bar, 25% Oxygen

Of the seven tests in this atmosphere, those for the three largest droplets were run on STS-83. It was observed from these three tests that[1] "in 25% oxygen, the lower peak temperatures have reduced the chemical rates to such an extent that flames of all sizes measured extinguished radiatively." In view of the fact that the initial droplet diameter was greater than 2 mm in these three runs, it is reasonable that the four runs on STS-94 focused on droplets having initial diameters less than 2 mm, since that serves to test whether any diffusive extinctions can occur in this atmosphere. Indeed, the results revealed that these smaller droplets extinguished diffusively instead of radiatively, as may be seen from Fig. 4, thus establishing the boundary between diffusive and radiative extinction as varying from initial droplet diameters of perhaps 4 mm at 32% oxygen (Fig. 2) to about 3 mm at 30% oxygen (Fig. 3) to about 2 mm at 25% oxygen (Fig. 4).

Since it is known that radiative extinction can occur even after the flame diameter has reached a maximum value and has begun to decrease,[1,5] and since diffusive extinction occurs at easily measurable, non-zero flame diameters, it can be difficult to distinguish between the two modes of extinction solely on the basis of flame-diameter histories. Figure 4 demonstrates a better way to make this distinction for heptane droplet combustion, namely on the basis of the droplet-diameter history. Radiative extinctions occur at a substantially large droplet diameter, and continued vaporization of the liquid in the hot atmosphere is evident in the droplet-diameter histories after radiative extinction, but with diffusive extinction the heptane droplet diameters are always very small at extinction, and the droplet is often not visible after extinction. The droplet diameters at extinction, reported in Table 1, are all close to the limit of the droplet-view resolution; in the richer atmospheres they are too small to be measured, and even in the leaner atmospheres there is substantial uncertainty in the values reported.

For diffusive extinctions, in which the droplet disappears very near the time of flame extinction, an interesting question concerns whether the flame extinguishes before or after the droplet disappers;[1] both situations are possible theoretically. Comparison of results for runs 15 and 16 in Figs. 4 and A4 suggests that both types of behavior may be possible. These two droplets had very nearly the same initial diameter, but the initial flame diameter was clearly smaller in run 16. In this run (16) the flame definitely extinguished before the droplet disappeared; on the other hand, in run 15, with a large initial flame diameter, it appears that the flame may have persisted slightly longer than the droplet. The coordination of timing between the flame and droplet views is accurate enough that it is not the main source of uncertainty in these conclusions; instead, the main uncertainty is introduced through the droplet-view spatial-resolution limitation which makes it difficult to ascertain exactly when the droplet disappears. If both types of behavior indeed occur in Fig. 4, then it can be concluded that the initial condition affects whether the flame or droplet disappears first, a result that could occur because the time-dependent behavior in the outer zone allows its entire history to depend on the initial conditions. A greater amount of pre-ignition vaporization, giving a larger initial flame diameter, could cause the flame to last longer than

the droplet. This degree of uncoupling between flame and droplet is associated with the near-quasisteady droplet behavior and the strong time-dependent influences on the flame. Theoretical analyses aimed at improving explanations of these effects evidently should focus on influences of different amounts of initial energy deposition. It is seen here that the initial condition at ignition may exert qualitative effects even at extinction.

Since the droplet view was not available in test 17, the initial droplet diameter was estimated from the camcorder view, as was also done for the other two tests listed in Table 1 that lack droplet views. There is substantial uncertainty in these camcorder readings; indeed, the initial droplet diameter in test 17 may well have been less than that in test 18, as the corresponding flame-diameter data would suggest. The measured burning rate for test 18, listed in Table 1, is appreciably higher than for any other test in this atmosphere, as would be expected from convective effects on this rapidly moving droplet. The flame in this test clearly lasts longer than the droplet, as might be expected from the large amount of vaporization that would occur as the droplet bounces off the igniter wire.

Initial and final burning-rate constants are not given in Table 1 for this atmosphere because curvatures in quasisteady diameter-squared plots were not detectable in this weaker atmosphere. Curvatures clearly decrease with increasing dilution of the atmosphere.

Results at 1.00 Bar, 20% Oxygen

All four tests at normal atmospheric pressure in the oxygen-helium atmosphere containing 20% oxygen, shown in Fig. 5, were obtained on STS-94. Results at this lowest oxygen concentration are noticeably different from those in other atmospheres. First, it should be observed that the traces extend for only two seconds, the flames not even persisting that long. Although the slopes of the diameter-squared curves appear to be small because of the short time period, the burning-rate data in Table 1 indicate rate constants quite comparable with those at the other oxygen contents. The tests cover a wide range of initial droplet diameters and show very small final droplet diameters for the two smallest droplets but appreciably large final diameters for the two largest droplets. The flame-diameter histories are peculiar and also qualitatively different for the largest and smallest droplets, increasing with time until extinction for the largest droplets and always decreasing with time for the smallest. At first glance, it may seem that the two largest droplets experience radiative extinction and the two smallest diffusive extinction, but further study raises questions concerning this interpretation.

An important observation is the absence of any correlation between droplet and flame time histories in Figs. 5 and A5. This suggests that the droplet is not responding to any flame behavior but instead is merely vaporizing under the influence of the energy deposited in the ignition process, during the brief period recorded. The different vaporization-rate constants of different droplets, then, would mainly reflect different amounts of initial energy deposition, thereby accounting for the somewhat irregular variation of burning rate with droplet size, shown in Table 1. The inward motion of the flames of the two smaller droplets merely reflects the gradual consumption of fuel vapor formed during the ignition process, while the outward motion for the larger droplets could be due to additional vaporization, a greater influence at larger droplet size. With this interpretation, all of the extinctions are caused by energy loss having an appreciable radiative component in this atmosphere. The atmosphere would be considered as not having a sufficient amount of oxygen to support quasi-steady droplet combustion. The 20% condition, then, would be beyond a flammability limit for droplet combustion, the brief periods of flame existence, always less than 1.5 seconds, being a consequence only of the initial energy deposition.

This second interpretation appears to be the more convincing one. It implies that, in this atmosphere, even the smallest droplet tested, namely one with an initial diameter of only about 0.9 mm, is large enough to lie beyond the boundary of radiant extinction. The time scales are sufficiently short that this tentative conclusion can be explored further in drop-tower testing. No drop-tower experiments have yet been performed in this atmosphere.

Results at 0.50 Bar, 40% Oxygen

All of the tests at 0.50 bar were run on STS-94. Fairly complete ranges of oxygen contents and initial diameters were studied at this pressure, enabling pressure dependences to be inferred from comparisons with results obtained at 1.00 bar.

Only one test was completed at 40% oxygen, the richest atmosphere investigated. From the results, shown in Figs. 6 and A6, it is seen that diffusive extinction occurs and that the diameter-squared plot exhibits curvature like that seen at 1.00 bar and 35% oxygen. Since the initial droplet diameter in this test is rather large, it may be concluded that diffusive extinction may be expected for all accessible initial droplet diameters in this atmosphere. This behavior is consistent with that found at 1.00 bar 35% oxygen; reduction of the total pressure by a factor of two is more than offset by the 5% increase in oxygen concentration of the atmosphere.

Results at 0.50 Bar, 35% Oxygen

Four tests were obtained in this atmosphere, as seen in Figs. 7 and A7. As indicated in Table 1, a wide range of initial droplet diameters was explored, although the droplet view was unavailable for the smallest droplet. The droplet-view traces in this atmosphere, as well as in 40% oxygen, are more irregular than in other atmospheres. A tendency towards this kind of "noisy" behavior also was found in 35 and 32% oxygen at 1.00 bar and is caused by soot particles interfering with the droplet-diameter data reduction. Sooting was less intense in lower-oxygen environments and did not degrade droplet-diameter data in any of the helium-oxygen atmospheres at 30% oxygen and below. The irregularity in the 0.50 bar 35% oxygen tests prevented possible curvatures in diameter-square plots from being detected, and such curvatures did not occur at 30% and below, thus demonstrating that at a given oxygen concentration the curvature effects are noticeably less at the lower pressures. In fact, at lower pressure and lower oxygen, small curvature begins to occur in the opposite direction, consistent with what has been predicted and observed in air in drop-tower tests with smaller droplets.

For the two largest droplets in this atmosphere, both the flame and the droplet drifted out of the field of view after about 3 to 5 seconds. It is, therefore, not possible to determine from the data whether these flames would experience radiative or diffusive extinction. Figure 1 demonstrated that at 1.00 bar for this oxygen concentration all droplets experienced diffusive extinction. The present data at 0.50 bar clearly demonstrates diffusive extinction for the two smaller droplets, and comparison of the results for test 26 with those for tests 2 and 3 reveals that the 2.1 mm droplet at 0.50 bar exhibits burning-time and flame-diameter behavior intermediate between those of the 1.9 and 2.9 mm droplets at 1.00 bar. Burning-rate constants in Table 1 for 0.50 bar at this oxygen content are less than those for 1.00 bar, but there is no clear indication of any qualitative differences in behavior. Thus, it seems quite possible that all of the droplets burned in this atmosphere at 0.50 bar would experience diffusive extinction, just as they did at 1.00 bar, even though the drift of the two larger droplets prevents drawing a definite conclusion. The influence of pressure on the droplet-combustion behavior thus appears to be weak.

Results at 0.50 Bar, 30% Oxygen

The four tests at 0.50 bar in 30% oxygen, shown in Figs. 8 and A8, span a narrower range of initial droplet diameters. The range nevertheless appears to be sufficient for demonstrating the different types of combustion behavior that occur in this atmosphere—the largest droplet is seen to experience radiant extinction, while the two smallest droplets exhibit diffusive extinction. Consequently, the boundary between radiant and diffusive extinction in this atmosphere must occur at an initial droplet diameter between 2 and 4 mm, which is comparable with what was found at 1.00 bar with this same oxygen concentration. Comparison of Figs. 3 and 8 reveals that, aside from the smaller burning-rate

constants at the lower pressure, the principal difference is that, for a given initial droplet diameter, flame extinction occurs sooner at the lower pressure. This is consistent with a decrease in chemical reaction rates with decreasing pressure. Despite this pressure effect on the burning time, the data are insufficient to establish any clear pressure dependence of the boundary between radiant and diffusive extinction.

The data, as a whole, do reveal systematic dependences of burning-rate constants on conditions. There are, however, some irregularities in the data, such as test 29, which showed an abnormally small burning-rate constant. This may be due to failure to capture an appreciable portion of the history of this test, for which the droplet and flame both soon leave the field of view. Irregularities such as this will be excluded in later evaluations of burning rates, where attention will be limited to the data having the greatest confidence.

Tests 30 and 31 suggest that diffusive extinction may occur before or after droplet disappearance, as previously remarked in connection with results of tests 15 and 16.

Results at 0.50 Bar, 25% Oxygen

There was only one test in this, the most dilute atmosphere at 0.50 bar. As seen in Fig. 9, however, it was a good test that clearly exhibited radiative extinction. Results of this test are best compared with those of test 14, a similarly sized droplet at 1.00 bar. They both experienced radiant extinction, and again, the extinction occurs somewhat earlier at the lower pressure. Another difference is that the maximum flame diameter is somewhat larger at the lower pressure; this systematic effect can also be seen by comparing corresponding tests in 30% oxygen for Figs. 3 and 8. Except for these quantitative differences, however, the behaviors at 0.50 and 1.00 bar are quite similar.

Results for 0.25 Bar

Results of the 0.25-bar tests, listed in Table 1, are shown in Fig. 10. In 50% oxygen, only the flame view was captured, and in Fig. 10 the flame diameter of this test is multiplied by a factor of two to avoid confusion with the droplet-diameter curve of the other test; this multiplication was considered unnecessary in the raw data of Fig. A10. The flame in this rich atmosphere exhibited diffusive extinction, as expected, and appeared to burn somewhat longer than flames of similarly sized droplets in other atmospheres, possible because of slower combustion at the lower pressure.

The droplet burned in 35% oxygen at this pressure exhibited radiative extinction. This is noteworthy because no radiative extinctions were seen in 35% oxygen at higher pressures. It thus implies that a pressure dependence of the boundary between radiative and diffusive extinction does exist, such that the boundary moves to higher oxygen percentages at lower total pressures, as might be expected. While the test implies the existence of this trend, data are insufficient for determining the pressure dependence of the boundary.

DCE Results at 1.00 Bar in Air

Figure 11 shows results of the four DCE air tests. Corresponding FSDC tests are given in Appendix B. The flames are much dimmer in this atmosphere than in the helium-oxygen atmospheres, and this dimness led to inaccuracies in recording flame diameters, especially for the larger droplets and for the two fiber-supported (tethered) droplets, giving rise to some irregularities seen in Figs. 11 and A11. Along with the dimmer flames, less soot was evident in this atmosphere than in the helium-oxygen atmospheres having oxygen concentrations of 30% or greater. Sooting behavior was discussed previously for helium-oxygen atmospheres,[1] and the general soot behavior for free droplets in air is similar to that in helium-oxygen. Many soot particles are visible in the backlit droplet views of the air tests, the number

being intermediate between that found in 25 and 30% oxygen in the helium-oxygen tests. A peculiarity of the observed soot dynamics in the two tests of tethered droplets in air is that the soot moves towards the fibers and thence towards the droplet, usually changing direction and retreating rapidly from the droplet surface when very near that surface (probably in response to the higher fuel-vapor outward flow velocity there), but occasionally apparently penetrating into the droplet. The motion towards the fiber and towards the droplet could well be driven by thermophoretic forces. Ring-like vortices of soot thus tend to be formed around the fiber.

One purpose of making measurements with both free and tethered droplets is to investigate the possible influences of the tethering on the combustion behavior. Tests 35 and 36 serve this objective well because their initial droplet diameters are very nearly identical. General agreement may be seen in that the two droplet-diameter traces are nearly indistinguishable, and the two flame-diameter histories are roughly similar; this supports the general usefulness of tethered-droplet experiments for drawing conclusions about free-droplet combustion. There are, however, a number of differences in detail, beyond the soot behavior, that are worth emphasizing.

First, as seen from the burning rates listed in Table 1, the tethered droplets have burning-rate constants that are more than 10% larger. Preliminary calculations given in Appendix C suggest that this may be due to additional heat input to the droplet by conduction along the fiber supports in the DCE tests. Such heat input may also tend to generate bubbles of fuel vapor in the liquid during combustion. Bubbles are not initially seen in the DCE tethered-droplet experiments but become evident several seconds into the burn and appear to grow throughout the tests, escaping in the final frames. Since internal bubble growth will decrease the measured rate of decrease of droplet diameter, the true burning-rate constants of the tethered droplets, in so far as their mass-loss rates are concerned, may well exceed those of free droplets by 20% or more. Interpretations of burning-rate measurements therefore need to consider possible influences of bubbles in the liquid. Bubble formation could also influence curvatures in diameter-squared plots, which are small in these experiments but tend to be in the same direction as those found in the helium-oxygen atmospheres at the higher oxygen contents.

Second, combustion of the tethered droplets seems to exhibit events in which the flame diameter increases abruptly in the middle of the burn. This behavior is evident in tests 35 and 37 in Figs. 11 and A11 and is clear visually, where the increase is associated with apparent jets of flame that shoot across the droplet field of view in a nonspherical manner. These have been suggested to result from soot-particle combustion or from residual fuel leaking from needles but may also be due to release of fuel vapor from the interior of the droplet, the vapor being formed by the heat input along the fiber supports. Although it was not possible to correlate this behavior in time with observed changes in the liquid in the droplet view, it is possible that such changes would be beyond the limit of detection. The tethered droplets thus exhibit greater irregularities in combustion behavior that may be traced to influences of the fiber support.

Extinction events were less clear for the tethered droplets because of the dimness of the flame. The dimness was so severe for the larger of the two tethered droplets that the flame could no longer be detected after about 10 seconds of burning, even though it was clear from the droplet-diameter trace that combustion was continuing. This effect is responsible for the end of the flame-diameter data for test 35 in Figs. 11 and A11. The smaller free and fiber-supported droplets clearly exhibited diffusive extinction, but because of the poor resolution and free-droplet drift, it was not possible to ascertain whether diffusive or radiative extinction occurred for the two larger droplets in these experiments. For the two smaller droplets, the droplet diameter at extinction was too small to be measured, possibly zero for the free droplet, but the flame diameter at extinction could be determined for the free droplet and is given in Table 1. Where entries are absent in Table 1, flame data are unavailable because of dimness, and droplet data are unavailable because extinction times are unknown and bubbling associated with fiber interactions causes data to be very irregular and unreliable. The FSDC experiments provide further information relevant to these tests.

FSDC Experiments

The FSDC experiment was designed to fit into the so-called "glovebox" facility in Spacelab. The general characteristics and operation of the experiment have been described previously.[6] Color cameras for both a flame view and a droplet view were provided, both operating at 30 frames per second. Backlight for the droplet view was supplied by a row of red light-emitting diodes (LED's) which produce good resolution of the droplet image. The blue flame, however, could not be detected by the flame-view camera. This camera did, however, record glowing of the support fiber where the flame intersected the fiber, and attempts were made to estimate the flame diameter from the location of the fiber glow. The fiber glow typically revealed the initially increasing flame diameter, but the glow usually became undetectable shortly after combustion began, being obscured by other lighting. It therefore was not possible to obtain useable flame-diameter data for these heptane droplet tests in quiescent atmospheres, and only droplet-diameter data are reported here. This flame-view difficulty was less severe for other fuels and for heptane combustion in convective flow; FSDC data for other tests therefore provide flame information.

Similar to the tethered DCE tests in air, the FSDC experiments involve deploying the droplet onto the fiber from two opposed needles and employ hot-wire ignition in Spacelab cabin air. Unlike the automated DCE sequencing, however, the deployment and needle retraction are accomplished manually in FSDC by the operator in Spacelab, and by then pressing an ignition button the operator causes a single hot-wire loop (not two as in DCE) to move to a predetermined ignition position and to be energized electrically; after ignition is visually ascertained, the operator releases the ignition button, causing the hot-wire to retract and deenergize. The tethering fiber was a Nicalon ceramic fiber wire 80 μm in diameter for FSDC, in contrast to the Textron SCS-9A silicon-carbide fiber (also 80 microns in diameter) employed in DCE. The Nicalon wire, which is made by Dow Corning, is composed of 58% silicon, 31% carbon, and 11% oxygen; further properties of the wires are discussed in Appendix C. In the FSDC experiments on STS-73 the droplets were often observed to move along the fiber during burning. To eliminate this motion, in the STS-94 flight of FSDC analyzed here, the fiber was provided with a ceramic epoxy bead, 390 μm high and 670 μm wide, located at the center of the deployment and designed to anchor the droplet at the desired position. The bead also was important for tests with forced convection to fix the droplet location, and a number of experiments with two droplets burning simultaneously were performed, requiring multiple beads on the fiber. The FSDC and DCE experiments in air thus differed by the presence of the bead in the former.

To analyze the FSDC images, an AOI was defined at the top and bottom of the droplet (the left and right sides contained the fiber). Thresholding, as described for the DCE tests, was used. To clarify the images an AOI was defined to encompass the entire droplet, then an adaptive contrast stretching histogram was performed, followed by a Sobel edge detection and an extraction of the red LED color plane. The area AOI was not used for a diameter measurement with the FSDC data because the wire added extra measured area that was not part of the droplet. The reported diameters, therefore, are not averages of several diameter measurements, as in DCE, but instead are the single diameter measured orthogonal to the wire. Previously[6] the formula $(d_t^2 d_p)^{1/3}$ was used for the diameter estimate, where d_t is the diameter transverse (orthogonal) to the fiber and d_p is the diameter parallel to the fiber; in the present paper d_p was not recorded because of uncertainty in the measurements. From estimates based on previous[6] and present data, the diameter reported here may therefore be smaller, on the average, by about 10 to 15%, depending on the initial droplet diameter. The difference in the transverse and parallel diameters increases as the droplet volume decreases, and the ratio of the diameters approaches that of the bead.

Because of the bead and the manual deployment, it was more convenient to work with larger droplets in FSDC than in DCE. Droplet diameters ranged from about 3 to over 6 mm, in contrast to the 1 to 4 mm range of DCE. Initial droplet diameters in the range of 3 to 4 mm, thus, were investigated in both experiments. For heptane droplets in quiescent atmospheres, fifteen FSDC runs were completed and are analyzed here, as reported in the following section. The general characteristics of the combustion resembled those of the two tethered DCE runs in air; for example, both exhibited initially pure liquid droplets that developed bubbles shortly after ignition, as discussed previously. The bubbling was more

severe in FSDC than in DCE, possibly because of the presence of the bead, and the bubbling is responsible for irregularities in recorded droplet-diameter histories. It may be worth remarking that heptane droplets exhibited more severe bubbling than any other FSDC tests. This may be attributable to the higher flame temperature (leading to greater rates of energy input, for example through absorption of radiation by the bead) and lower boiling point of heptane, the greater volatility of the liquid favoring bubbling. The bubbling usually caused the droplet to dance about the bead for a portion of the combustion history, oscillating irregularly in position until the bead occupied a significant part of the spherical volume. Bubble bursting was not observed, possibly because of the low burning rate or, perhaps more likely, because of vapor escape from the interior along the fiber. Even though bursting was not observed, most tests show a sudden change in diameter due to bubble dynamics. This change generally occurs near the end of the test when the bubble occupies most of the droplet volume. In test 53, however, a bubble forms early, grows rapidly, and causes a change in diameter less than half-way through the test, at about 2.5 seconds; then, another bubble forms (or perhaps some of the vapor from the first bubble remains), grows, and causes a second change in diameter about 5 seconds into the test. Another similarity of the FSDC and tethered DCE tests is the presence of flame jets visible in some, but not all, of the droplet views. Soot particles could be seen with the backlight, moving in a vortex-like motion as previously described. Sometimes they were deposited on the fiber, and, on occasion in its dancing motion along the fiber, the droplet captured a deposited soot particle and carried it away.

Results of FSDC tests

The results of the FSDC tests that were analyzed are shown as raw data in Appendix B. At the end of Appendix B is a graph containing all the FSDC tests analyzed for this paper; this graph shows the similarities in droplet history (and, hence, burning rate) in different tests, indicating the repeatability of results. Table 2 summarizes the numerical results along with the corresponding DCE results for air.

To aid comparisons with the DCE data, the FSDC droplet traces in Appendix B start at the approximate time of ignition. Ignition is always strongly visible in the flame view, but the GMT in these experiments was accurate only to 1 second; consequently, ignition in the droplet view is based on the visual evidence in that view. To gauge accuracy, the number of frames between deployment and ignition of several tests was counted in both views. Start times were found to agree within 0.2 seconds or less in the two views.

The traces in Appendix B all show fairly linear diameter-squared plots. In most cases this behavior continues to a very small diameter, not much different from the bead diameter. This type of behavior is consistent with diffusive extinction but is not consistent with radiative extinction, which occurs with larger final droplet diameters and causes the evaporation rate to decrease, as indicated earlier. Tests 39, 40, and 42 have traces that end at large droplet diameters, which seem to indicate radiative extinction. There is no indication of extinction at the time the traces end, however; tracking was unable to continue because of dimness similar to that suffered in the flame views of the DCE air tests. Consequently, it may be concluded that radiative extinction did not occur in the FSDC tests with heptane. Since initial droplet diameters in these tests were as large as 6 mm, larger than the initial diameters in any of the DCE tests in air, it seems unlikely that radiative extinction could have occurred in any of the air tests in DCE. The tethered droplets have an additional heat input resulting in higher burning rates and, possibly, additional fuel vaporization. It is conceivable that large free droplets in air could experience radiative extinction, while the additional vaporization in the tethered experiments delays extinction. The experiments that have been performed in these flights, however, do not establish the occurrence of radiative extinction in air; they only establish a limit on the droplet diameter, on the order of 2 mm for free droplets and 6 mm for FSDC tethered droplets, below which the extinction is definitely diffusive.

It is of interest to compare results of different types of tests in air for droplets of approximately the same initial diameter. Tests 35, 36, and 52 are of particular note in this respect, since they all have similar initial droplet diameters and encompass the three types of air tests—untethered DCE, tethered DCE and FSDC. The burning-rate constant is higher for FSDC, and the DCE tethered test has a larger

burning-rate constant than the untethered one. The increase in the burning-rate constant for FSDC may be due to the bead on the fiber, which artificially inflates the droplet diameter, or it could be within the normal variation from test to test. A comparison of burning-rate trends suggests the latter since test 52 is at the upper limit of normal variation and test 35 is at the lower limit. The bead therefore may not affect the burning rate appreciably more than the presence of the fiber seems to increases the burning rate.

The burning-rate summary in Table 2 includes all tests in air. It is seen from this summary that average burning rates tend to be somewhat smaller (10 to 20%) for large droplets (possibly because of greater radiant energy loss) and somewhat smaller (again 10 to 20%) for free droplets, as opposed to tethered droplets, possibly because of added heat input to the liquid along the fiber. The results also show small but measurable curvatures in diameter-squared plots, as may be seen by comparing initial and final burning-rate constants. Differences tend to be on the order of 20%, less than found in the helium-oxygen mixtures of low dilution but usually in the same direction, that is, higher burning-rate constants initially. There is little difference between free and tethered droplets in this respect, both possibly preferentially accumulating species of lower volatility, but there is greater test-to-test variation in the tethered experiments (one of which shows the lowest burning-rate constant initially) as a consequence of variability associated with droplet-fiber interaction.

Extinction Diameters

Theories have been developed for calculating droplet diameters at extinction, termed extinction diameters. Different theories are based on different assumptions concerning chemical kinetics and droplet combustion processes. Measurements of droplet diameters at extinction are useful for comparison with theoretical predictions of extinction diameters. Table 1 lists all of the data obtained on droplet extinction diameters. Some of this data is plotted in Fig. 12 to illustrate trends.

When diffusive extinction occurs, droplet diameters at extinction are very small, usually too small to be measured and quite possibly often zero. There are seven entries in Table 1 in which droplet diameters at extinction are too small to be measured, that is, less than a limit of resolution between about 0.05 and 0.5 mm, depending on the experiment. Only three entries in Table 1 report measurable droplet extinction diameters for diffusive extinction. On the other hand, for radiative extinction, the droplet extinction diameters are much more readily determined. Excluding the tests in 20% oxygen for the reasons discussed previously, four droplet diameters at extinction are reported in Table 1, all of which are also plotted in Fig. 12.

From the data in Fig. 12 for 1.00 bar and 25% oxygen, through which the curve is drawn, it is seen that in this atmosphere the droplet extinction diameter increases with increasing initial droplet diameter. This trend is consistent with theoretical estimates for radiative extinction. For diffusive extinction with the flame in the quasisteady region, if the liquid fuel remains pure then the droplet diameter at extinction theoretically is independent of the initial droplet diameter;[7] the available data are insufficient to test this prediction. Although no significant functional dependencies for diffusive extinction could be measured, trends were obtained for radiative extinction. The point at 1.00 bar and 30% oxygen in Fig. 12 suggests a decrease in the droplet radiative extinction diameter with increasing oxygen concentration at a given pressure and initial droplet diameter, while that at 0.50 bar and 25% oxygen indicates an increase in the droplet radiative extinction diameter with decreasing pressure at a given oxygen mole fraction and initial droplet diameter. Both of these trends are expected from the dependence of the reaction rate on pressure and oxygen concentration.

In contrast to droplet diameters at extinction, substantial data were acquired on flame diameters at extinction in helium-oxygen atmospheres. Indications are that flames always extinguish at flame diameters large enough to be measured. Since fewer theoretical predictions have been made of these flame extinction diameters (final flame diameters), additional theoretical work may be pursued for making comparisons with the present experimental results, which are listed in Table 1 and partially plotted in Fig. 13.

The solid curves in Fig. 13 correspond to 1.00 bar and the dashed curves to 0.50 bar; these are the pressures at which most of the data were obtained. From the three solid curves it is evident that, in general, the final flame diameter increases as the oxygen mole fraction decreases—a behavior expected from the dependence of the chemical reaction rate on the oxygen concentration. The solid curves show that the final flame diameter also tends to increase with increasing initial droplet diameter. The rate of this last increase is greatest in the middle of the region of radiant extinction, as theory suggests, but the increase also occurs for diffusive extinction, as the curve for 1.00 bar and 35% oxygen demonstrates (since in this atmosphere all extinctions were diffusive). Classical totally quasisteady theory would give extinction flame diameters independent of initial droplet diameters, contrary to the experimental results in 35% oxygen. The flame therefore cannot be entirely quasisteady at extinction; it must be at least partially in the outer non-quasisteady zone. At sufficiently small initial droplet diameters the final flame diameter is independent of the initial droplet diameter, within experimental uncertainty, suggesting that quasisteady conditions may be approached at these small sizes. It is of interest that the results for the solid curve at 25% oxygen show a tendency for the final flame diameter to become independent of the initial droplet diameter at large initial droplet diameters as well, giving rise to an inflection in the curve; this may be a consequence of approaching a radiation-dominated ignition limit for these large droplets in this highly diluted atmosphere. Such inflections may occur in other atmospheres as well, although there are insufficient data to demonstrate it, and their characteristics may depend on finer details of the method of ignition, so that it is difficult to speculate on how these curves may behave at larger initial droplet diameters. At the smallest initial droplet diameters, it is somewhat surprising how closely the curves approach each other, the differences in final flame diameters in 30 and 35% oxygen being less than experimental variability; further study of the chemical kinetics of diffusive flame extinction would be needed to investigate this phenomenon.

Comparison of the solid and dashed curves in Fig. 13 reveals the influence of pressure on the final flame diameter. The general behaviors at the two pressures are quite similar for both 30 and 35% oxygen, and the point in Fig. 13 at 0.50 bar and 25% oxygen (test 32) is at least consistent with the qualitative behaviors being the same at this mole fraction as well. The final diameters at the lower pressure are, however, larger, as may be expected from the lower reaction rates. Just as the effect of oxygen concentration is relatively small for diffusive extinction and becomes much larger as radiative extinction begins (at increasing initial droplet diameter), so the pressure effect is comparatively small for diffusive extinction. The small final flame diameter in Table 1 at 0.50 bar and 40% oxygen (test 23) suggests that there is a definite dependence on oxygen mole fraction for diffusive extinction. Not plotted in Fig. 13 are the two data points in Table 1 for 0.25 bar (tests 33 and 34); these data (one for diffusive extinction and one radiative) are consistent with the same general behavior extending to this lower pressure as well. A fairly coherent picture of the characteristics of the flame diameter at extinction, as exemplified most clearly by the solid curves in Fig. 13, emerges from these results. Quantitative explanations await future theoretical investigations.

It is of interest to exhibit graphically the boundary between radiative and diffusive extinction, in a plane of oxygen mole fraction and initial droplet diameter for different pressures, as determined by these experiments. Figure 14 is such a plot, with the open symbols corresponding to observations of diffusive extinction and the closed symbols corresponding to radiative extinction. Figure 14 shows that, although there is considerable uncertainty about exactly where the boundary lies, the general direction and curvature of the boundary between the two regimes seems well defined. The error bars indicate the range of uncertainty of the boundary location at 1.00 bar; data are insufficient to distinguish differences in boundary locations at 1.00 and 0.50 bar.

Burning Rates

A summary graph of burning-rate constants as functions of initial droplet diameter is shown as Fig. 15, based on the data given in Tables 1 and 2. In this figure the solid curves pertain to helium-oxygen atmospheres at 1.00 bar, the dashed curves to helium-oxygen atmospheres at 0.50 bar and the dotted

curves to air. The general trend of a decrease in the burning-rate constant with increasing initial droplet diameter is evident in all of this data. Some specific data points, particularly the triangular points representing 1.00 bar and 25% oxygen and the circles representing 0.50 bar and 35% oxygen, suggest the existence of a minimum burning-rate constant at a particular initial droplet diameter, but in view of the general trends of most of the data, it seem likely that these minima are only apparent and are the result of run-to-run variability, although their existence cannot entirely be ruled out. The decreasing of the burning-rate constant with increasing initial droplet diameter is consistent with previous work,[8] where the change was attributed to the formation of larger quantities of soot.

Figure 15 clearly shows that the burning-rate constant decreases with increasing dilution, as expected. It seems noteworthy that the extent of this increase is much greater at 1.00 bar (solid curves) than at 0.50 bar (dashed curves). At 0.50 bar the results for 35 and 30% oxygen are very close together, and even the single point available at this pressure for 25% oxygen is quite close to these. Although there would be greater confidence in the conclusion that the dilution effect is small at 0.50 bar if more data were available at that pressure, there seems to be sufficient data to motivate seeking possible theoretical reasons for the small effect. No theoretical explanation is immediately apparent.

The results in Fig. 15 for air clearly show the increase in the burning-rate constant caused by the fiber support. The two untethered droplets definitely exhibited lower burning-rate constants, as remarked previously. The burning-rate constants for air are substantially lower than those for helium-oxygen mixtures because of the high thermal conductivity of helium.

Conclusion

The tests performed during MSL-1 led to the first documented radiant extinction in n-heptane droplet combustion. The main DCE results pertain to combustion in helium-oxygen atmospheres with ambient temperatures near room temperature. Tests performed at 1.00 bar showed that diffusive extinction occurs for droplets smaller than 4.1 mm burning in a 35% oxygen environment with helium as the inert. Diffusive extinction also occurs for droplets under 3.2 mm in a 30% environment and 1.7 mm in 25% oxygen. The 20% oxygen environment was shown to be unable to support the combustion of droplets larger than 0.9 mm in initial diameter. At 1.00 bar radiant extinction was observed for droplets over 3.9 mm in the 30% environment and 2.8 mm in the 25 and 20% environment. No tests at 35% in 1.00 bar exhibited radiant extinction (the largest droplet was 4.1 mm). For the 0.50-bar tests radiant extinction was observed during two tests: 3.1 mm initial droplet diameter in a 30% oxygen environment and 2.9 mm initial droplet diameter in the 25% oxygen environment. The 0.25-bar tests showed radiant extinction at 35% oxygen with an initial droplet diameter of 2.6 mm and diffusive extinction at 50% oxygen with an initial droplet diameter of about 1.5 mm. These results can be viewed graphically in Fig. 14 with an approximate radiant extinction limit drawn.

All of the droplets exhibited the classic linear decrease in time of the square of their diameter. This behavior occurred independent of the more complex flame behavior. Flames were generally found to grow and then shrink for tests that underwent diffusive extinction, and grow to a maximum diameter, occasionally shrinking slightly, in cases of radiant extinction. Some exceptions were found to this flame behavior, but all occurred during the 1.00 bar 20% oxygen tests, and they were assumed to result from combustion of the accumulated vapors only. In several environments the graphs of the square of the droplet diameter as a function of time exhibited a curvature wherein the burning-rate constant decreased over time. The lower oxygen environments, as well as the lower pressures, did not exhibit this curvature. The explanation of this phenomenon is still being explored.

Nonzero final flame diameters were measured in all tests that stayed within the view of the flame-imaging camera. The final flame diameters appear to be dependent on initial droplet diameter, especially in cases of radiative extinction. Additionally, several of these droplets (in the richer oxygen environments) have immeasurably small to zero final droplet diameters, while in others the droplet still exists when the flame extinguishes.

Burning rate is seen to vary with initial droplet diameter, pressure, and oxygen content. The burning-rate constant decreases with increasing initial droplet diameter. Additionally, the pressure and oxygen percentage have the predicted effect on burning-rate constants—decreasing the pressure or increasing the oxygen mole fraction increases the burning rate. More study of the influences of the initial droplet diameter remains to be completed because the cause of the decrease is not well understood.

These results provide valuable data with which to compare current theories. They demonstrate the usefulness of tethered tests for comparison with free-droplet behavior and show repeatability of results. These results have raised new questions and have shown the need for more research in certain areas. Further quantitative study of radiant extinction needs to be done, as does examination of final droplet and flame diameters with diffusive extinction.

References

1. Nayagam, V., Haggard, J.B., Jr., Colantonio, R.O., Marchese, A.J., Dryer, F.L., Zhang, B.L. and Williams, F.A., "Microgravity N-Heptane Droplet Combustion in Oxygen-Helium Mixtures at Atmospheric Pressure," *AIAA Journal*, Vol. 36, No. 8, August, 1998, pp. 1369–1378.
2. Marchese, A.J., Dryer, F.L., and Nayagam, V., "Numerical Modeling of Isolated n-Alkane Droplet Flames: Initial Comparisons with Ground and Space-Based Microgravity Experiments," Combustion and Flame, Vol. 116, No. 3, February, 1999, pp. 432–459.
3. Klimek, R.B., Wright, T.W., and Sielken, R.S., "Color Image Processing and Object Tracking System," NASA TM–107144, 1996.
4. Cleveland, W.S., "Robust Locally Weighted Regression and Smoothing Scatterplots," *Journal of the American Statistical Association*, Vol. 74, No. 368, pp. 829–836.
5. Fachini, F.F., Linan, A., and Williams, F.A., "Theory of Flame Histories in Droplet Combustion at Small Stoiciometric Fuel-Air Ratios," *AIAA Journal*, Vol. 37, No. 11, November, 1999, pp. 1426–1435.
6. Dietrich, D.L., Haggard, J.B., Jr., Dryer, F.L., Nayagam, V., Shaw, B.D., and Williams, F.A., "Droplet Combustion Experiments in Spacelab," *Twenty-Sixth Symposium (International) on Combustion*, The Combustion Institute, Pittsburgh, PA, 1996, pp. 1201–1207.
7. Card, J.M., and Williams, F.A., "Asymptotic Analysis with Reduced Chemistry for the Burning of n-Heptane Droplets," *Combustion and Flame*, Vol. 93, No. 4, June, 1993, pp. 375–390.
8. Avedisian, C.T., "Soot Formation in Spherically Symmetric Droplet Combustion," Physical and Chemical Aspects of Combustion, edited by F.L Dryer and R.F. Sawyer, Combustion Science and Technology Book Series, Vol. 4, Gordon and Breach Science Publishers, Amsterdam, 1997, pp. 148–160.
9. Shaw, B.D. and Harrison, M.J., "Asymptotic Analysis of Shapes of Fiber-Supported Droplets Burning in Reduced Gravity," paper 99F–29 presented at the 1999 Fall Meeting of the Western States Section of the Combustion Institute, UC Irvine, Irvine, CA October 25–26.
10. Struk, P.M., Ackerman M., Nayagam V., Dietrich D.L., "On Calculating Burning Rates During Fiber Supported Droplet Combustion," *Microgravity Science and Technology*, Vol. 11, No. 4, 1998, pp. 144–157.
11. Drivsky, W.A. and Schuhmann, R., Jr., "Derivation of Phase Diagram for the Silicon-Oxygen-Carbon System," *Transaction of the Metallurgical Society of AIME*, Vol. 221, October, 1961, pp. 898–904.
12. Ghosh, A. and St. Pierre, G.R., "Ternary Phase Diagrams for the Si-C-O System," *Transaction of the Metallurgical Society of AIME*, Vol. 245, September, 1969, pp. 2106–2108.
13. Zinkle, S.J. and Snead, L.L., "Thermophysical and Mechanical Properties of SiC/SiC Composites," http://www.fusion.ucla.edu/apex/pdfs/SiC.pdf, May 1998.
14. Touloukian, Y.S., ed., Thermophysical Properties of High Temperature Solid Materials, Vol. 55, Part 1, MacMillan Co., New York, 1967, pp. 123–129.
15. Saitoh, T., Yamazaki, K., and Viskanta, R., "Effect of Thermal Radiation on Transient Combustion of a Fuel Droplet," *Journal of Thermophysics and Heat Transfer*, Vol. 7, No. 1, January–March, 1993, pp. 94–100.
16. Chang, K. and Shieh, J., "Theoretical Investigation of Transient Droplet Combustion by Considering Flame Radiation," *International Journal of Heat and Mass Transfer*, Vol. 38, No. 14, 1995, pp. 2611–2621.

Table 1: Summary of experimental conditions and results for DCE

Test number	Pressure, bar	Oxygen, percent	Initial diameter, mm	Burn time, s	Burning-rate constant, mm^2/s			Extinction diameter, mm		Drift velocity, mm/s	
					Initial	Overall	Final	Flame	Droplet	Flame-view	Droplet-view
1[a]	1.00	35	3.93	14.13	1.81	1.26	1.13	8.43	[e]	2.06	1.54
2[a]	1.00	35	2.87	7.40	1.45	1.22	1.11	5.62	[d]	1.54	1.70
3[a]	1.00	35	1.91	3.07	1.47	1.35	1.00	4.63	[d]	3.86	4.17
4	1.00	32	3.87	[e]	1.50	1.10	0.92	[e]	[e]	1.43	0.71
5	1.00	32	2.92	[e]	1.71	1.23	0.93	[e]	[e]	2.21	2.26
6	1.00	32	2.72	7.70	1.55	1.19	1.03	5.08	[d]	1.81	1.62
7[a]	1.00	30	3.87	9.87	1.25	1.00	0.76	23.97	2.23	1.24	1.09
8[a]	1.00	30	2.94	9.47	1.11	1.02	0.99	9.01	[e]	1.85	1.99
9	1.00	30	1.82	3.37	1.16	1.15	1.06	4.28	[d]	1.37	4.54
10	1.00	30	1.81	3.30	1.30	1.22	1.07	4.70	[d]	2.25	3.03
11	1.00	30	1.78	3.30	1.32	1.18	1.08	4.87	[d]	3.35	3.61
12[a]	1.00	25	4.01	8.80	[c]	0.99	[c]	25.54	[e]	1.54	1.62
13[a]	1.00	25	3.15	4.40	[c]	0.94	[c]	25.37	2.40	0.83	0.90
14[a]	1.00	25	2.75	4.80	[c]	0.93	[c]	21.24	1.77	1.03	1.12
15	1.00	25	1.68	2.83	[c]	0.96	[c]	9.96	0.60	1.70	2.66
16	1.00	25	1.61	2.53	[c]	0.95	[c]	9.28	0.61	1.57	3.53
17	1.00	25	1.18 ± 0.25[b]	1.67	[f]	[f]	[f]	6.74	[f]	3.57	[f]
18	1.00	25	1.12	[e]	[c]	1.10	[c]	[e]	[e]	3.57	28.45
19	1.00	20	3.71	1.30	[c]	1.00	[c]	31.80	3.69	0.93	[f]
20	1.00	20	2.77	1.27	[c]	1.15	[c]	25.90	2.60	1.43	1.89
21	1.00	20	1.36	0.90	[c]	1.03	[c]	11.70	0.81	5.34	0.82
22	1.00	20	0.89	0.43	[c]	0.85	[c]	10.20	0.65	12.90	12.10
23	0.50	40	3.26	11.30	1.52	1.16	0.98	3.64	[e]	2.51	2.56
24	0.50	35	4.00	[e]	[c]	1.01	[c]	[e]	[e]	1.74	2.84
25	0.50	35	3.60	[e]	[c]	0.78	[c]	[e]	[e]	4.83	4.62
26	0.50	35	2.09	4.67	[c]	0.98	[c]	6.48	[e]	2.26	4.11
27	0.50	35	1.18 ± 0.25[b]	1.70	[f]	[f]	[f]	6.27	[f]	11.20	[f]
28	0.50	30	3.08	6.57	[c]	0.91	[c]	26.20	[e]	1.60	[f]
29	0.50	30	2.68	[e]	[c]	0.50	[c]	[e]	[e]	9.36	8.13

Table 1: Summary of experimental conditions and results for DCE, concluded

Test number	Pressure, bar	Oxygen, percent	Initial diameter, mm	Burn time, s	Burning-rate constant, mm^2/s			Extinction diameter, mm		Drift velocity, mm/s	
					Initial	Overall	Final	Flame	Droplet	Flame-view	Droplet-view
30	0.50	30	2.26	5.43	[c]	0.93	[c]	9.75	[d]	2.35	2.80
31	0.50	30	2.23	4.90	[c]	0.92	[c]	12.00	0.73	3.64	2.18
32	0.50	25	2.86	2.83	[c]	0.85	[c]	27.70	2.42	1.88	1.76
33	0.25	50	1.5 ± 0.5[b]	2.87	[f]	[f]	[f]	3.47	[f]	7.40	[f]
34	0.25	35	2.61	6.57	[c]	0.90	[c]	26.20	[e]	1.67	2.39
35[h]	1.00	Air	3.10	18[g]	0.57	0.56	0.44			~0[g]	~0
36	1.00	Air	3.09	15.30	0.47	0.48	[e]	[e]	[e]	1.82	1.64
37[h]	1.00	Air	2.59	11.50	0.89	0.68	0.51			~0	~0
38	1.00	Air	1.68	6.03	0.68	0.66	0.53	3.77	[e]	1.47	1.64

[a]STS-83 test
[b]approximate value from the camcorder view
[c]not reported because variation is minimal
[d]not measurable, too small
[e]not measurable because of drift out of the field of view
[f]no droplet view
[g]approximate value estimated from very dim view
[h]tethered droplet

Table 2: Summary of results for combustion in air

Test number	Initial diameter, mm	Burn time, s	Burning-rate constant, mm^2/s		
			Initial	Overall	Final
FSDC					
39	6.60	[a]	0.60	0.50	[a]
40	5.82	58.80	0.65	0.53	0.50
41	5.71	[a]	0.46	0.51	[a]
42	5.47	[a]	0.55	0.55	[a]
43	5.40	55.40	0.58	0.51	0.51
44	4.82	37.50	0.59	0.55	0.36
45	4.65	39.50	0.54	0.56	0.48
46	4.60	36.70	0.72	0.56	0.50
47	4.41	32.80	0.66	0.54	0.45
48	4.31	32.00	0.66	0.54	0.47
49	3.58	18.20	0.72	0.71	0.50
50	3.58	19.40	0.81	0.68	0.50
51	3.34	18.50	0.78	0.62	0.47
52	3.10	11.50	0.80	0.77	0.63
53	3.07	5.50	1.81	1.69	0.86
DCE					
35	3.10	18.00	0.57	0.56	0.44
36[c]	3.09	15.30	0.47	0.48	[b]
37	2.59	11.50	0.89	0.68	0.51
38[c]	1.68	6.03	0.68	0.66	0.53

[a]dimness at the end of the test prevented measurement
[b]not measurable due to drift out of the field of view
[c]untethered (free) droplet

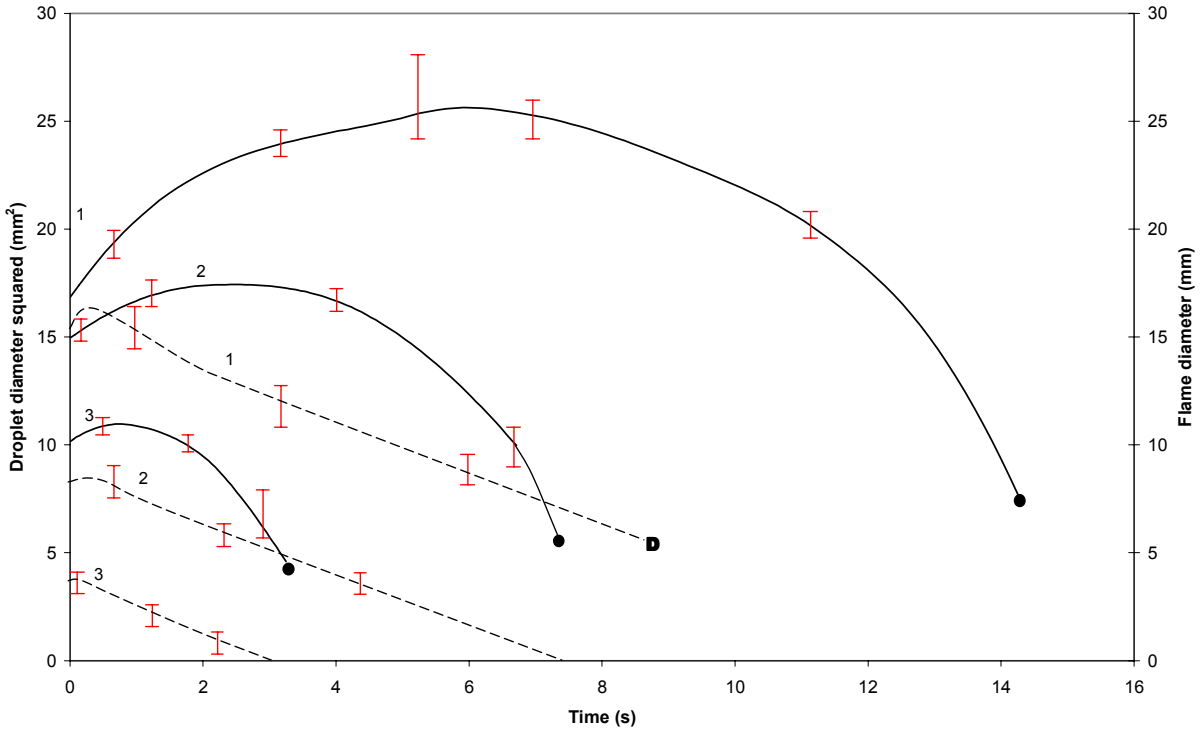

Figure 1: Smoothed graphs of droplet diameter squared and flame diameter as a function of time for an oxygen-helium environment at one bar and with a 35% mole fraction of oxygen.

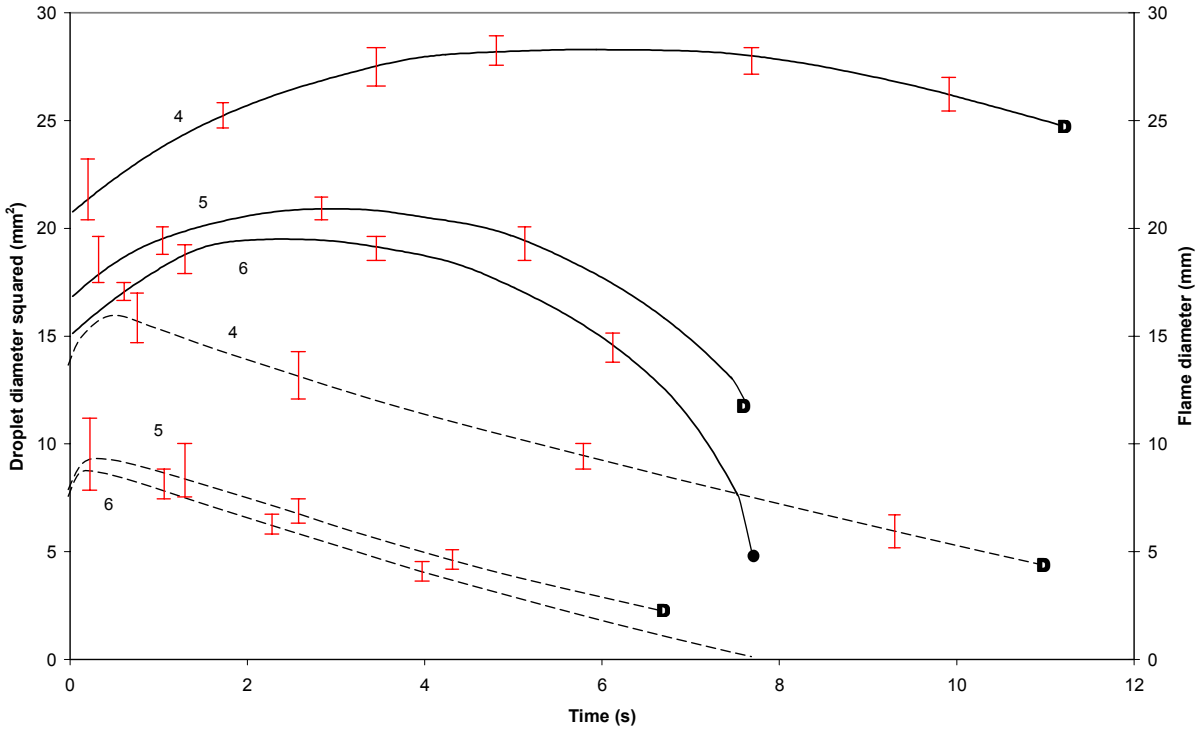

Figure 2: Smoothed graphs of droplet diameter squared and flame diameter as a function of time for an oxygen-helium environment at one bar and with a 32% mole fraction of oxygen.

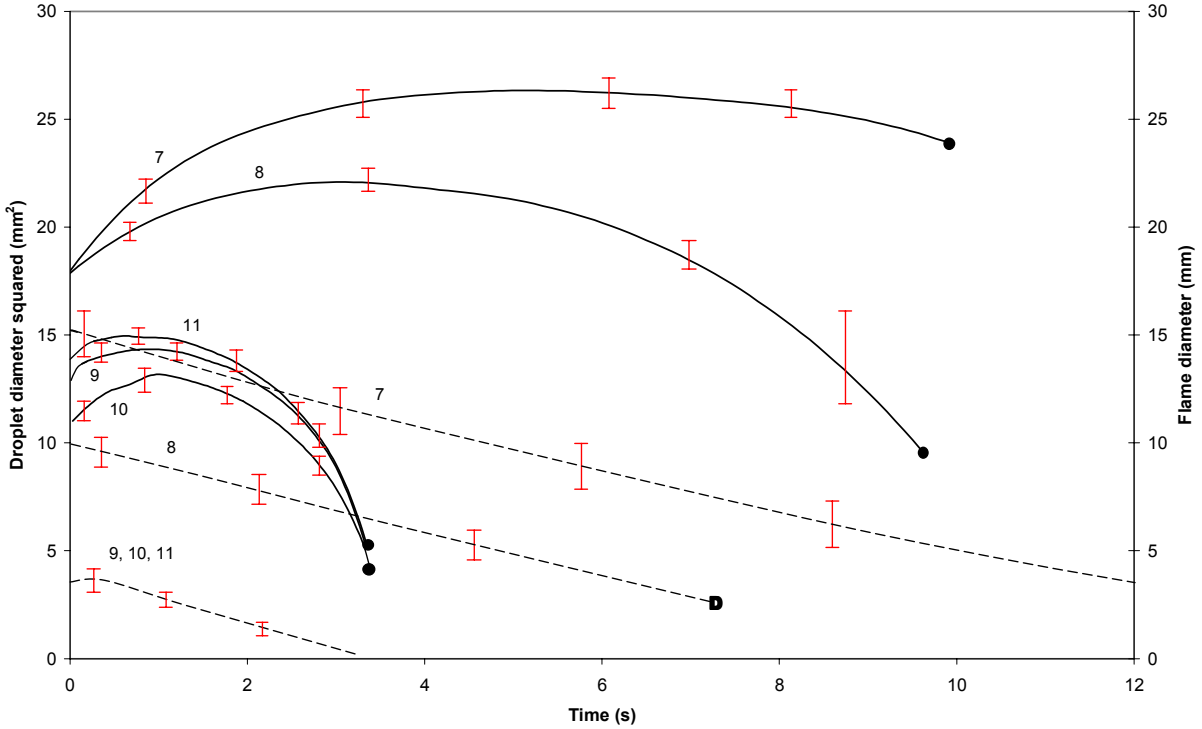

Figure 3: Smoothed graphs of droplet diameter squared and flame diameter as a function of time for an oxygen-helium environment at one bar and with a 30% mole fraction of oxygen.

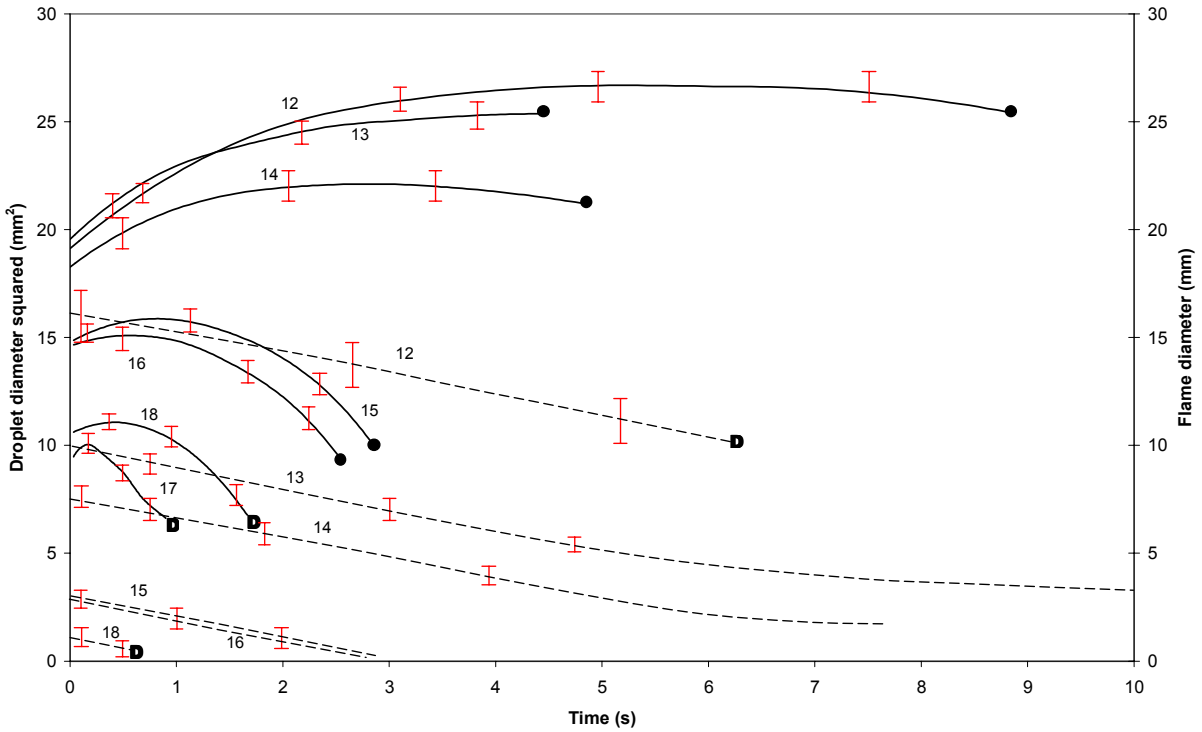

Figure 4: Smoothed graphs of droplet diameter squared and flame diameter as a function of time for an oxygen-helium environment at one bar and with a 25% mole fraction of oxygen.

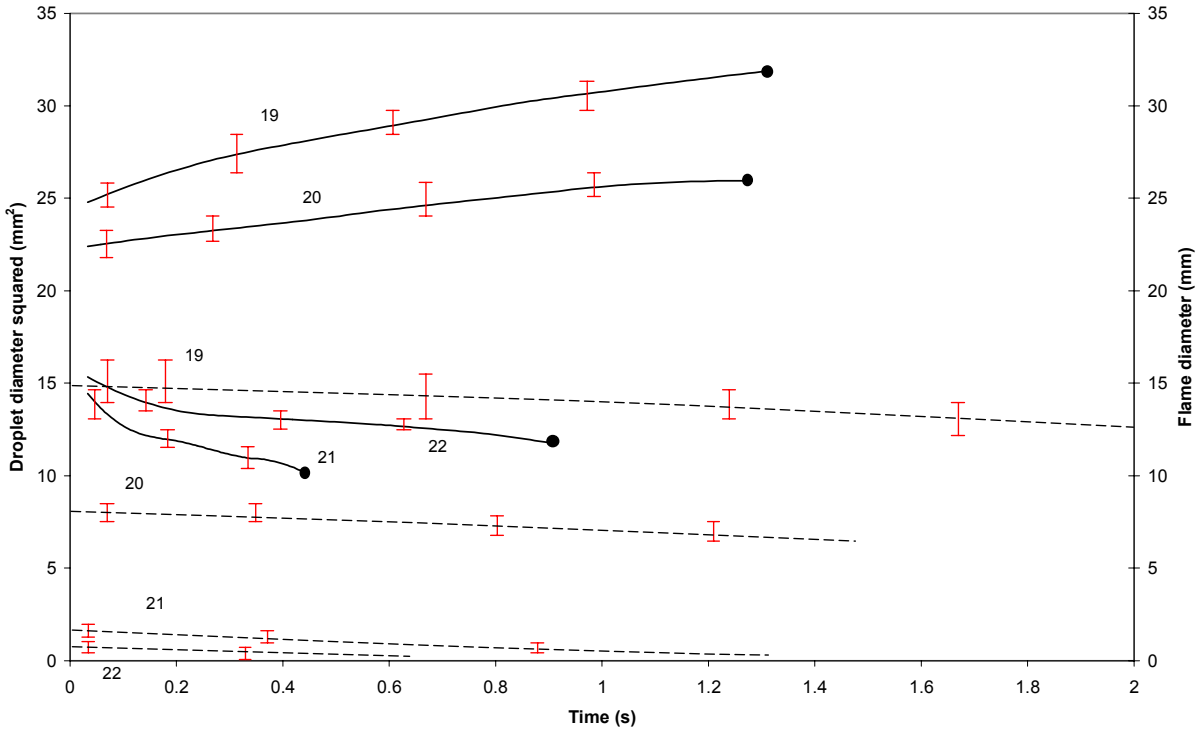

Figure 5: Smoothed graphs of droplet diameter squared and flame diameter as a function of time for an oxygen-helium environment at one bar and with a 20% mole fraction of oxygen.

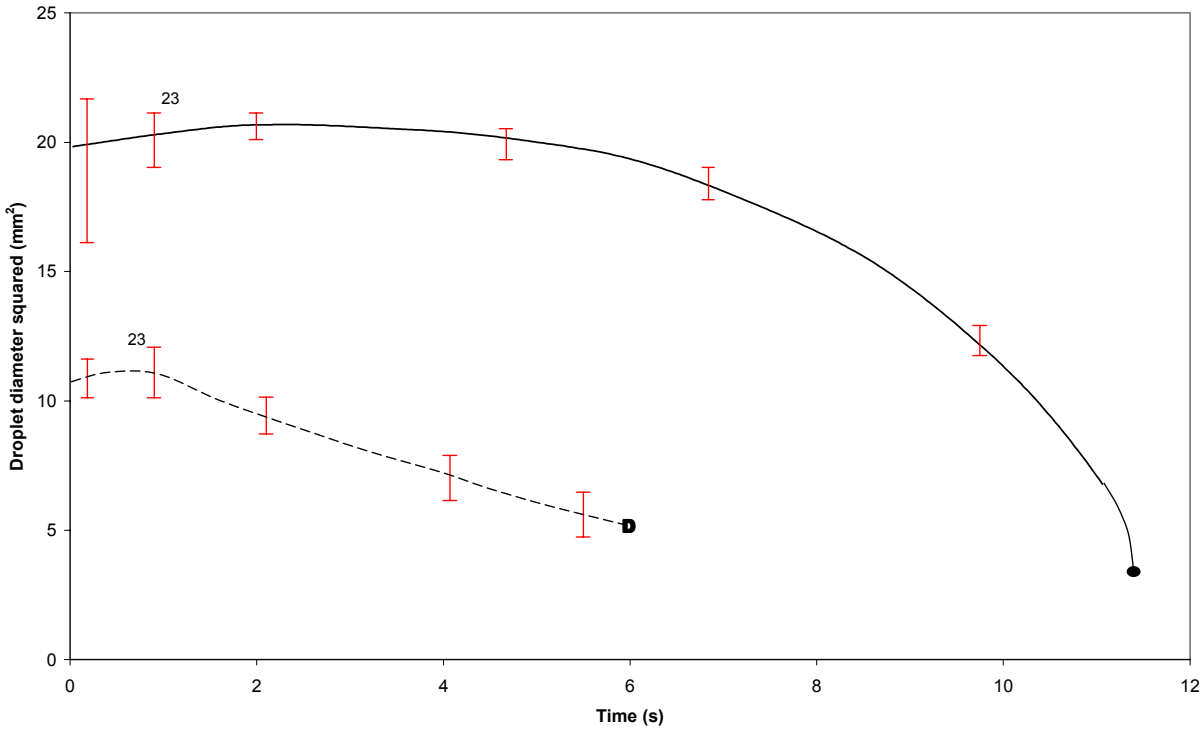

Figure 6: Smoothed graphs of droplet diameter squared and flame diameter as a function of time for an oxygen-helium environment at one-half bar and with a 40% mole fraction of oxygen.

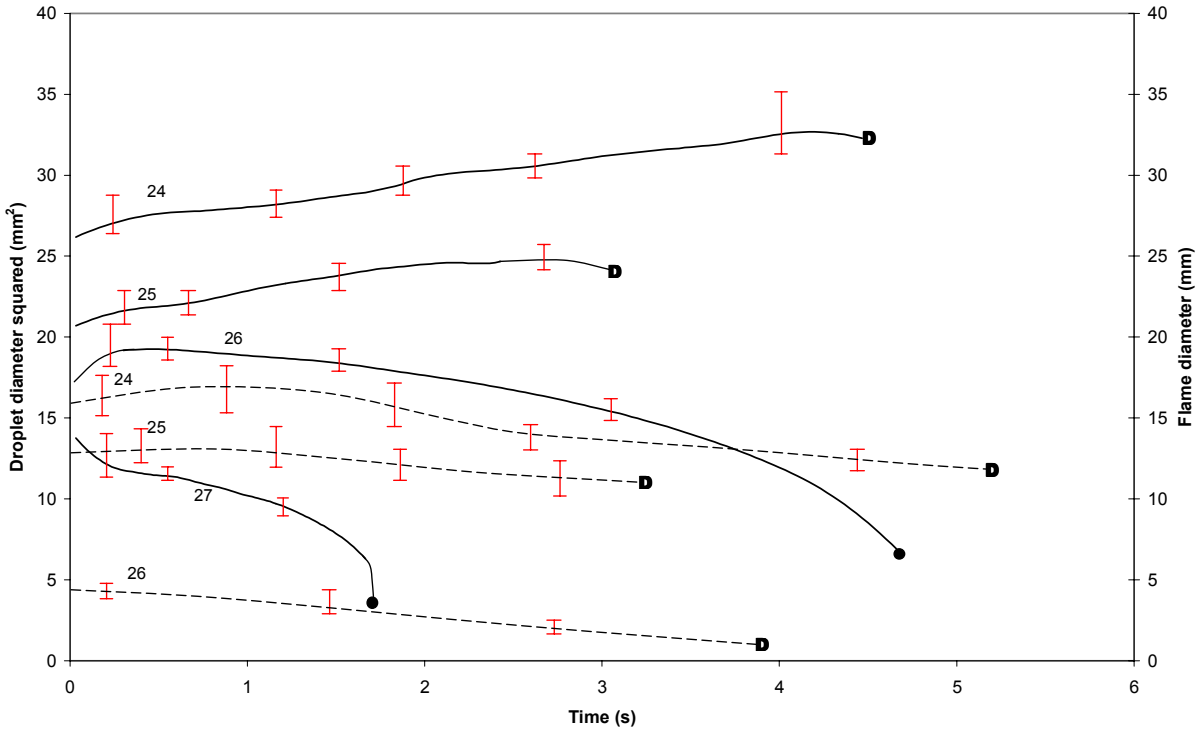

Figure 7: Smoothed graphs of droplet diameter squared and flame diameter as a function of time for an oxygen-helium environment at one-half bar and with a 35% mole fraction of oxygen.

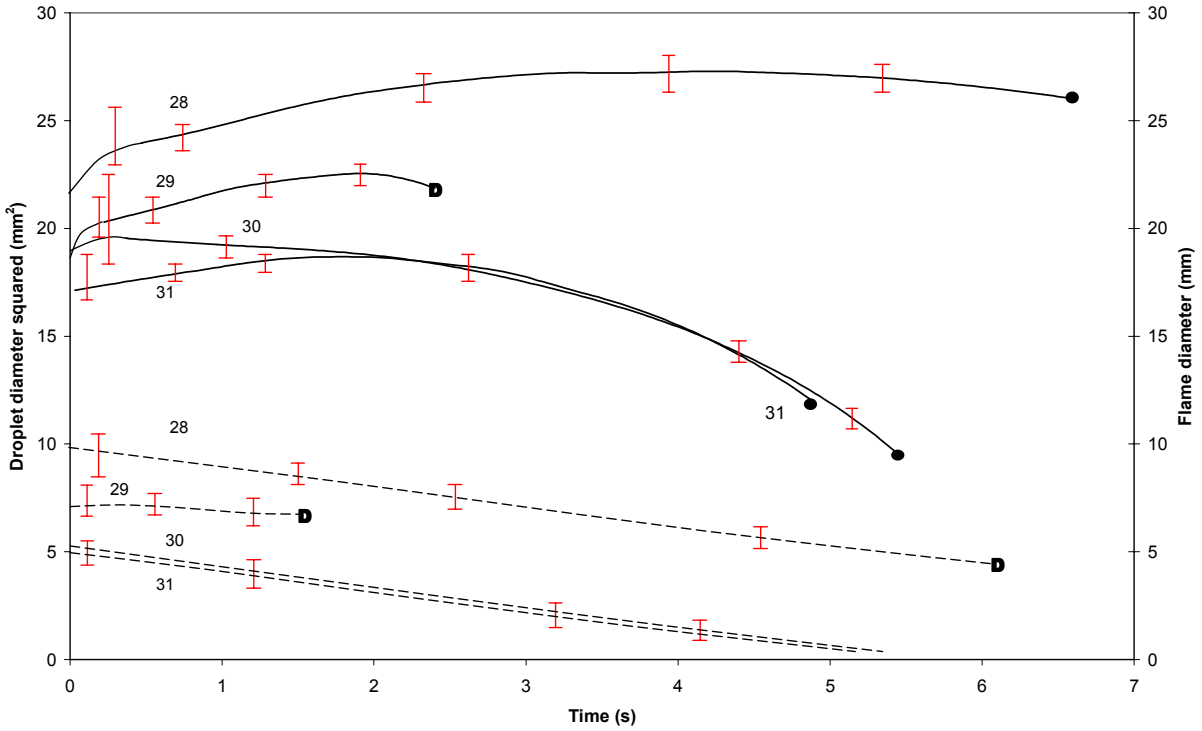

Figure 8: Smoothed graphs of droplet diameter squared and flame diameter as a function of time for an oxygen-helium environment at one-half bar and with a 30% mole fraction of oxygen.

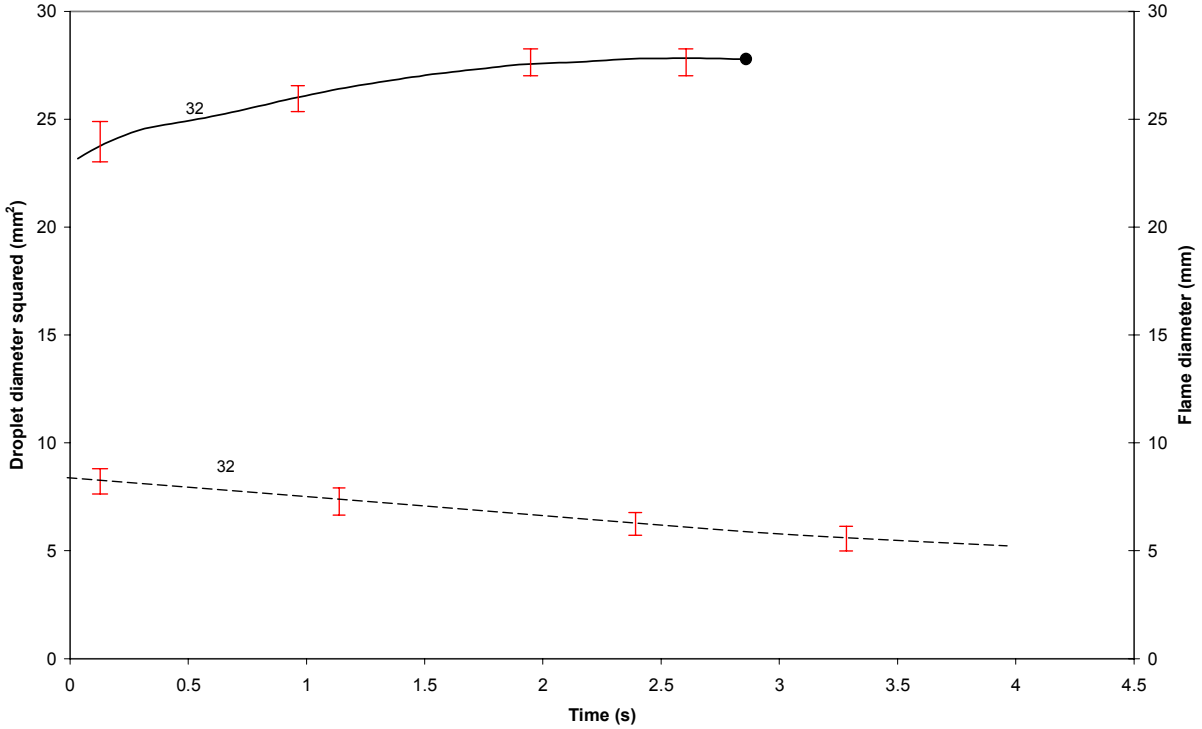

Figure 9: Smoothed graphs of droplet diameter squared and flame diameter as a function of time for an oxygen-helium environment at one-half bar and with a 25% mole fraction of oxygen.

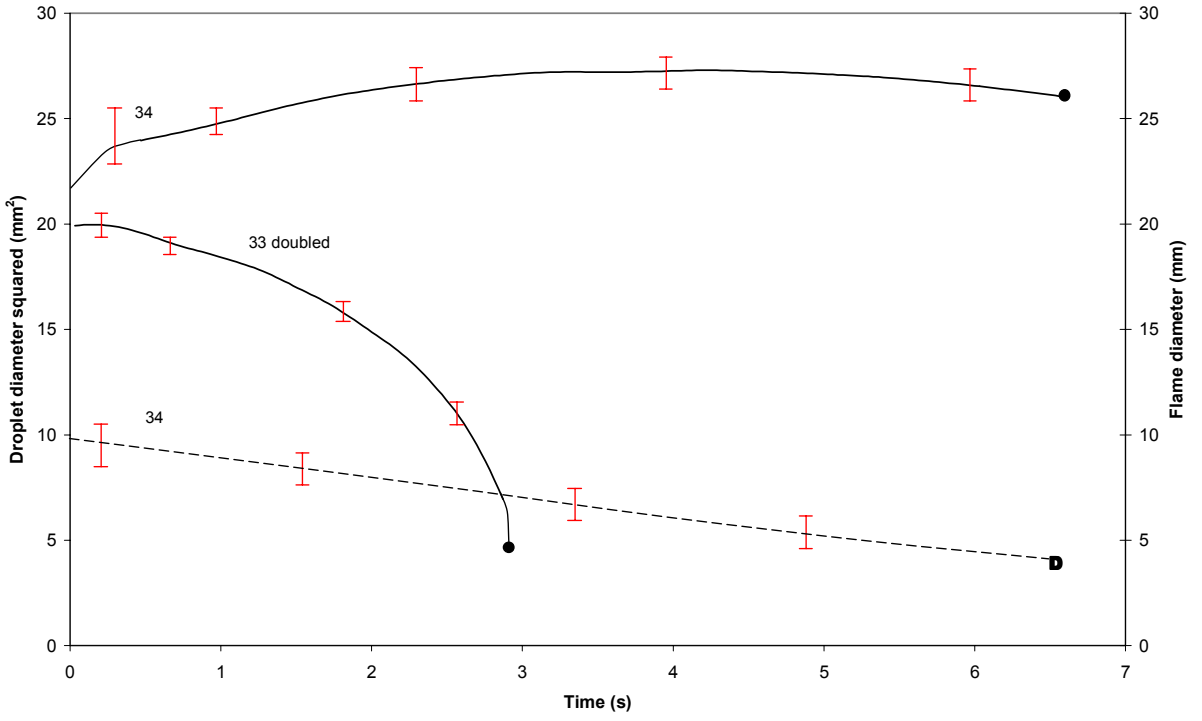

Figure 10: Smoothed graphs of droplet diameter squared and flame diameter as a function of time for oxygen-helium environments at one-quarter bar and with 35% or 50% mole fraction of oxygen.

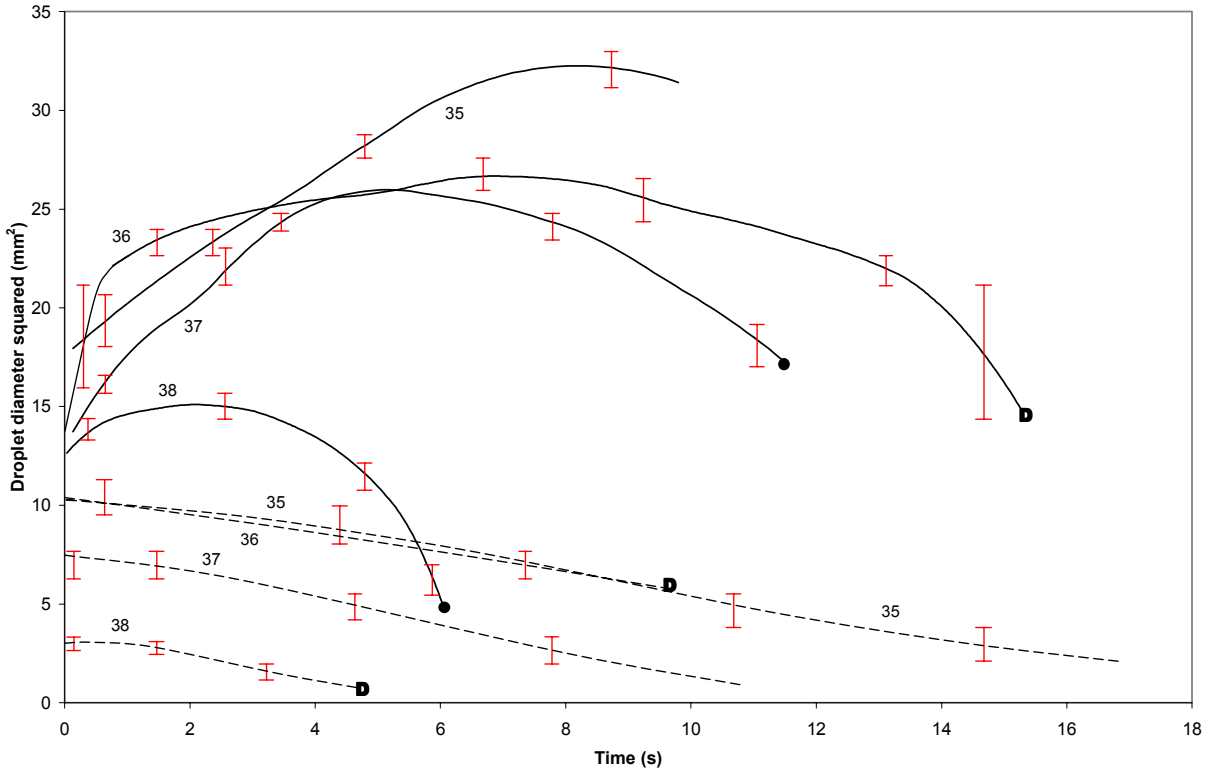

Figure 11: Smoothed graphs of droplet diameter squared and flame diameter as a function of time for an environment of cabin air at one bar.

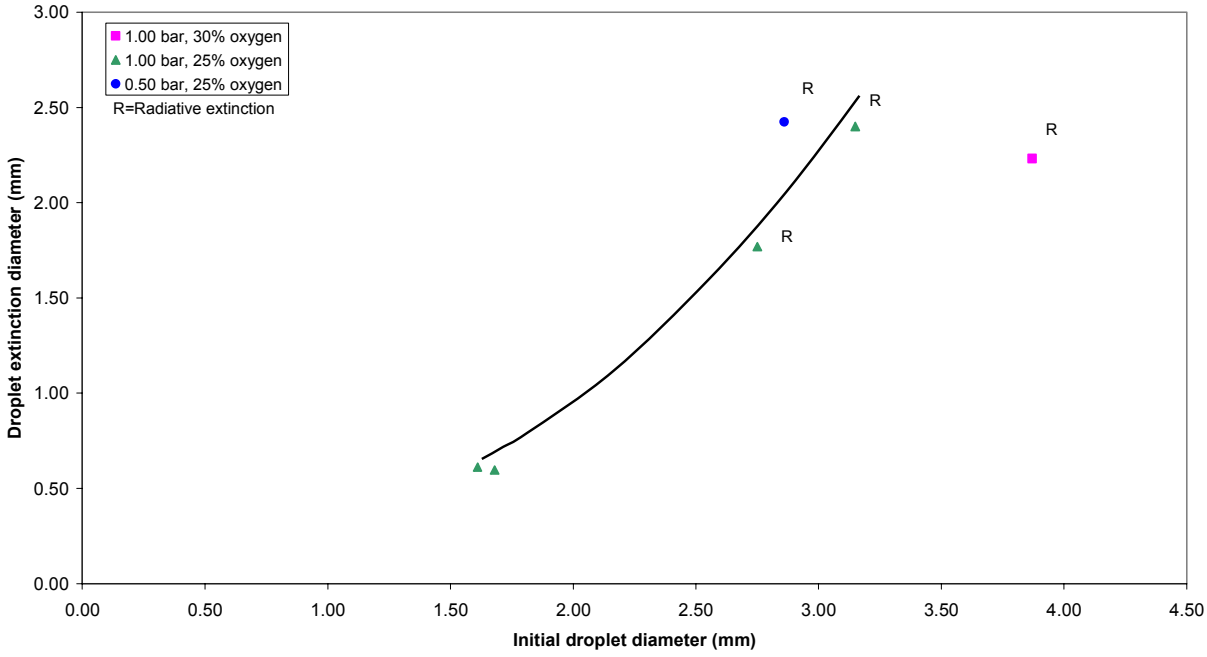

Figure 12: Droplet extinction diameter as a function of initial droplet diameter.

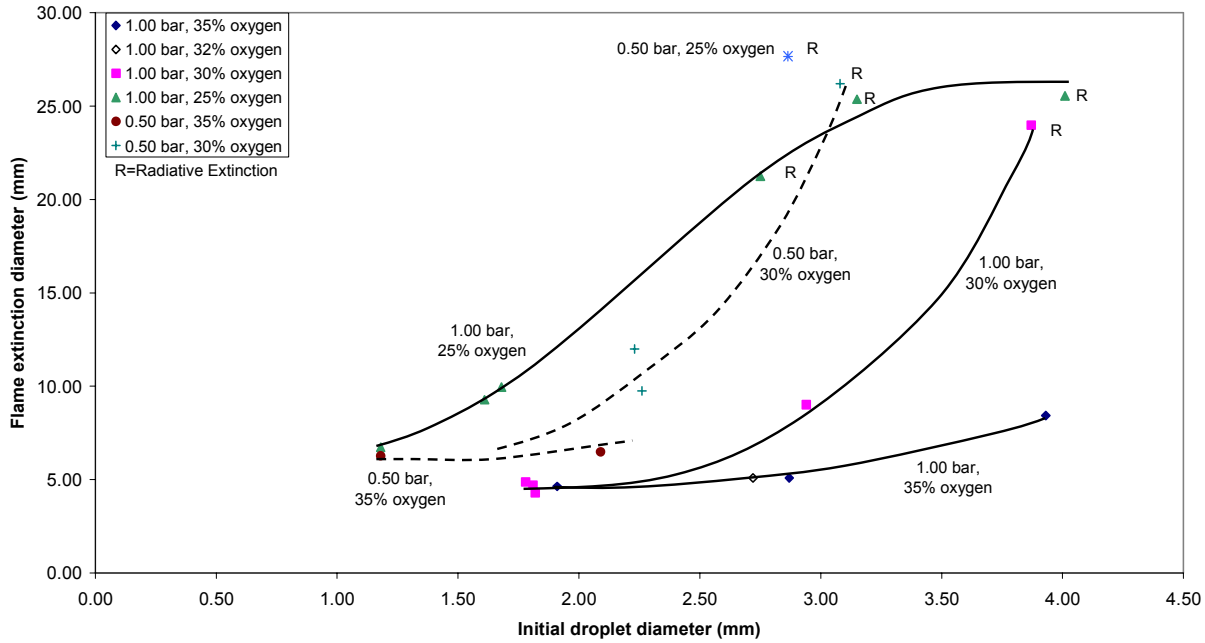

Figure 13: Flame extinction diameter as a function of initial droplet diameter.

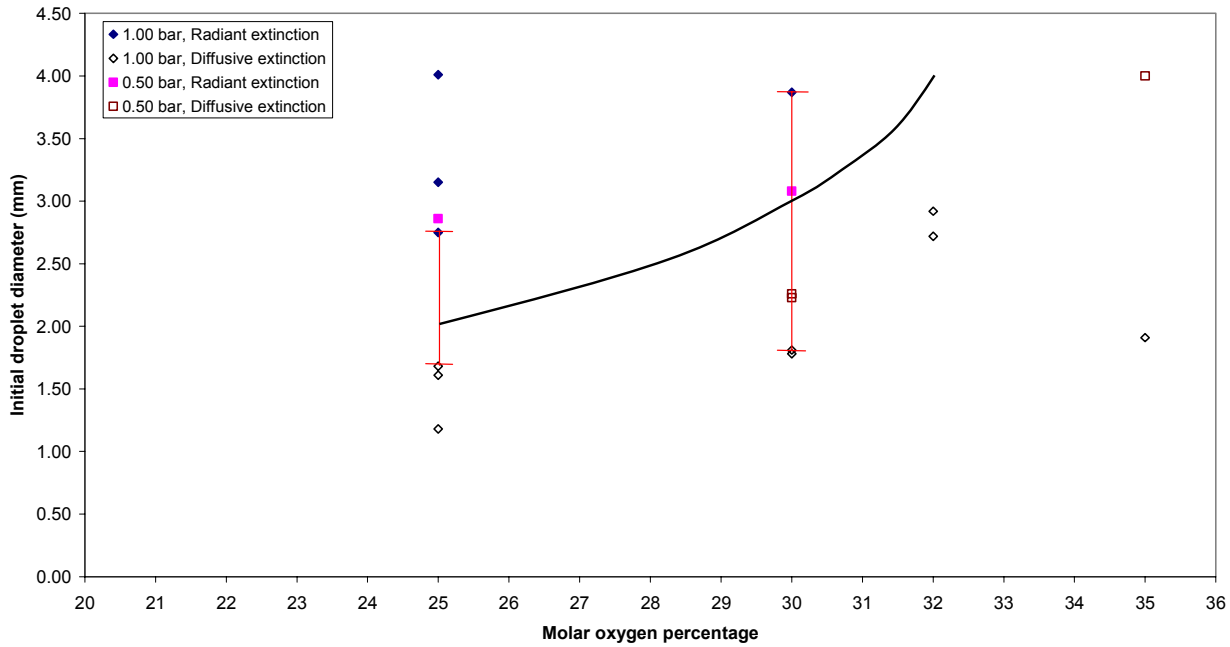

Figure 14: Proposed boundary between radiative and diffusive extinction in a plane of initial droplet diameter and molar oxygen percentage.

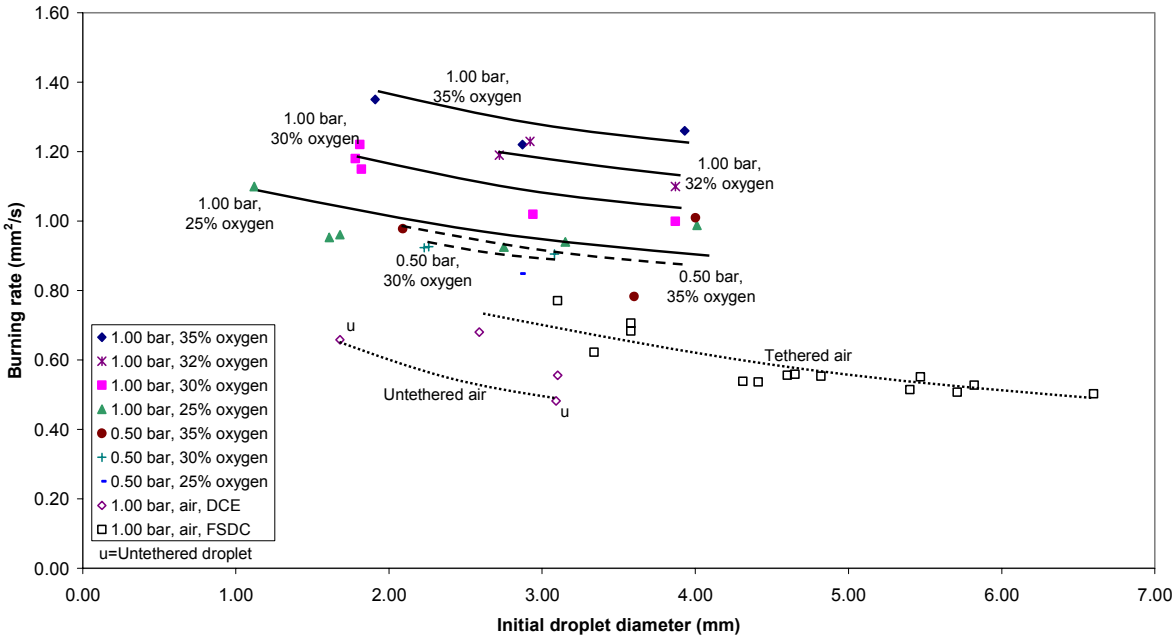

Figure 15: Burning rate as a function of initial droplet diameter.

Appendix A: DCE Data

This appendix presents the raw data for the DCE experiments. The numbering system is the same as in the main text and is summarized in Table 1. The methods of data reduction are described in the main text. Unlike Figs. 1 through 11 in the text, these graphs do not label the histories of droplets that drift from the field of view.

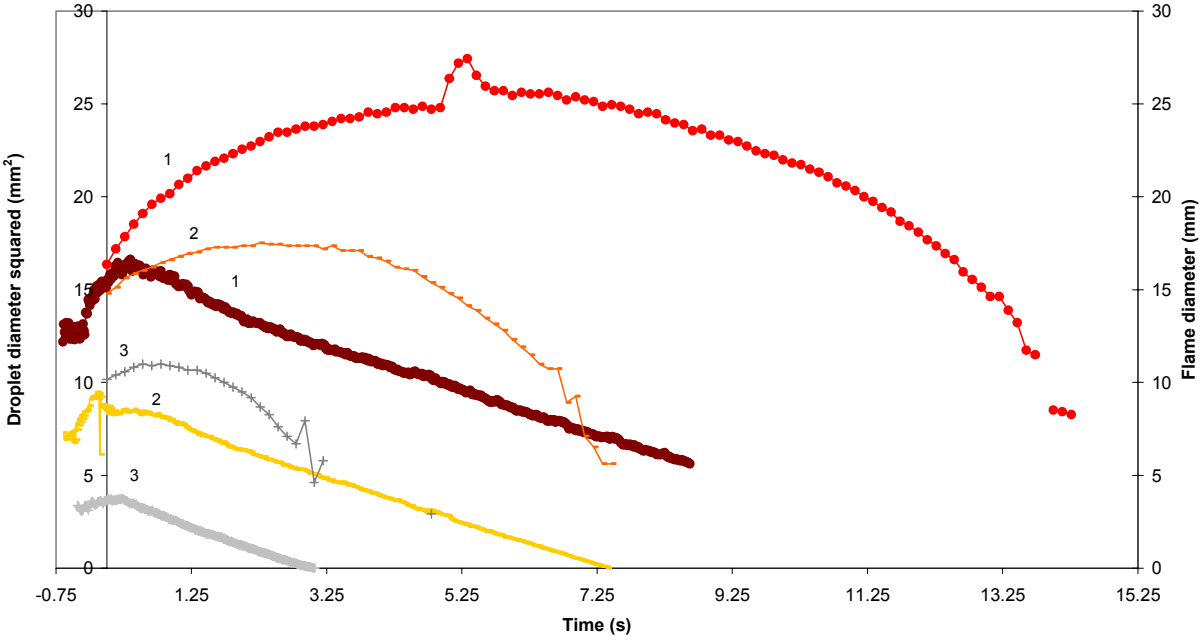

Figure A1: Graphs of droplet diameter squared and flame diameter as a function of time for an oxygen-helium environment at one bar and with a 35% mole fraction of oxygen.

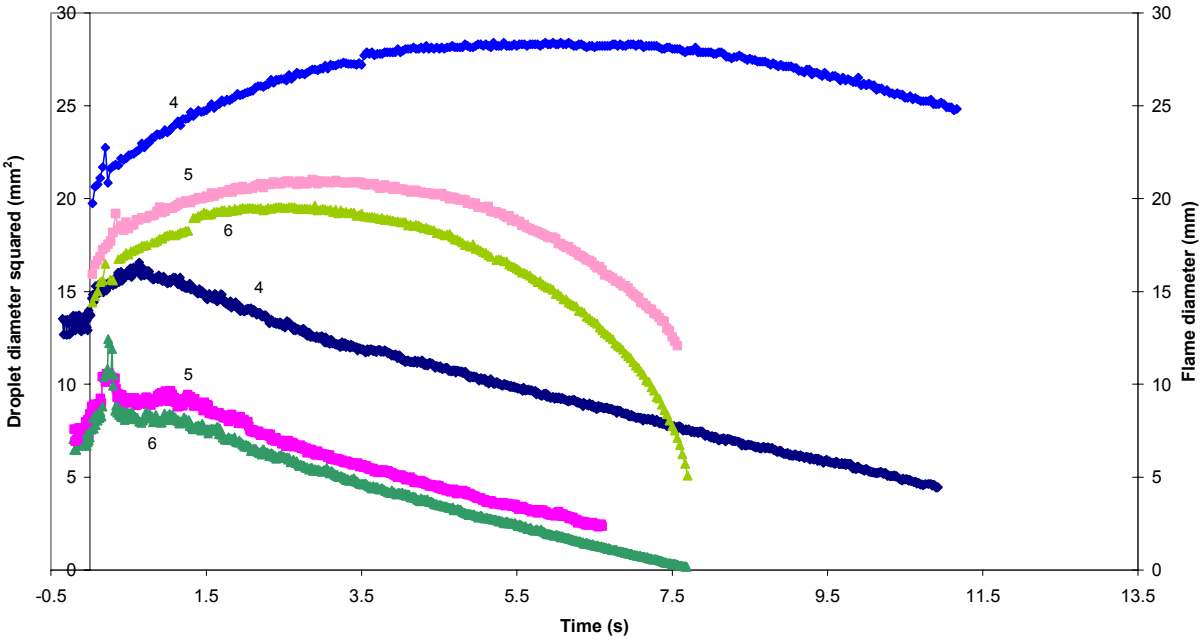

Figure A2: Graphs of droplet diameter squared and flame diameter as a function of time for an oxygen-helium environment at one bar and with a 32% mole fraction of oxygen.

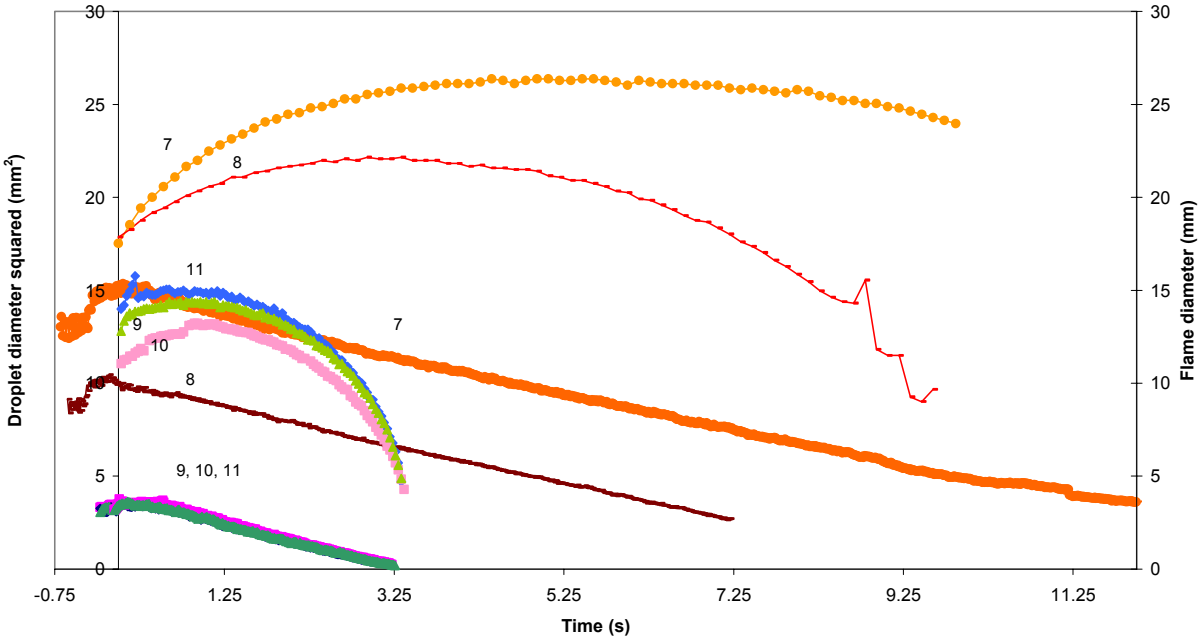

Figure A3: Graphs of droplet diameter squared and flame diameter as a function of time for an oxygen-helium environment at one bar and with a 30% mole fraction of oxygen.

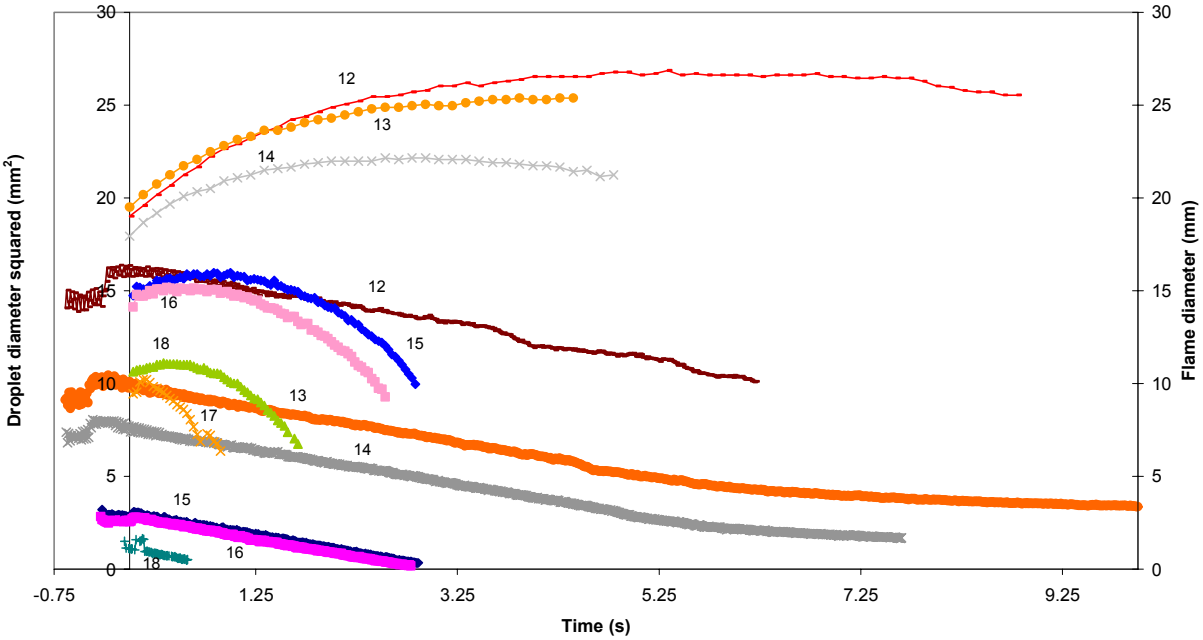

Figure A4: Graphs of droplet diameter squared and flame diameter as a function of time for an oxygen-helium environment at one bar and with a 25% mole fraction of oxygen.

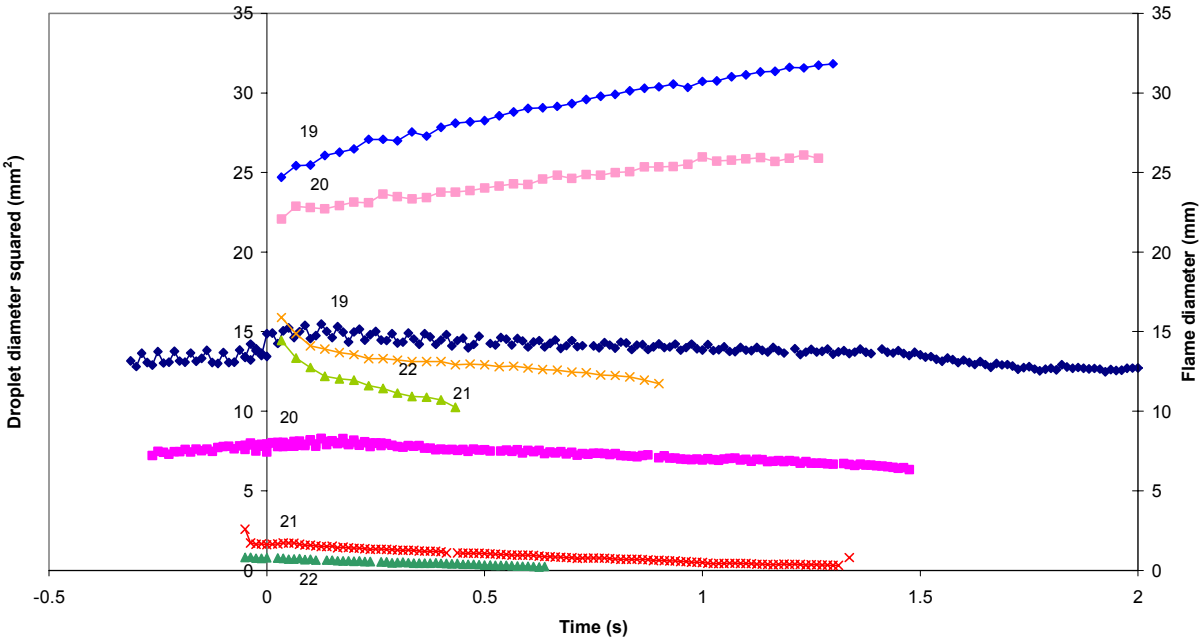

Figure A5: Graphs of droplet diameter squared and flame diameter as a function of time for an oxygen-helium environment at one bar and with a 20% mole fraction of oxygen.

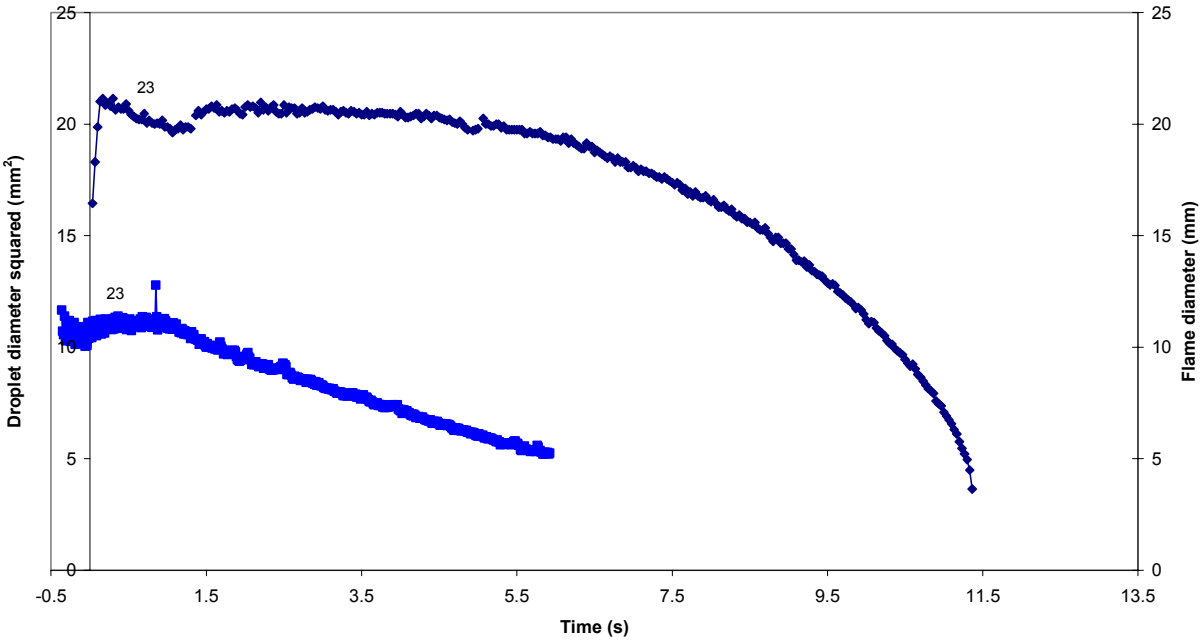

Figure A6: Graphs of droplet diameter squared and flame diameter as a function of time for an oxygen-helium environment at one-half bar and with a 40% mole fraction of oxygen.

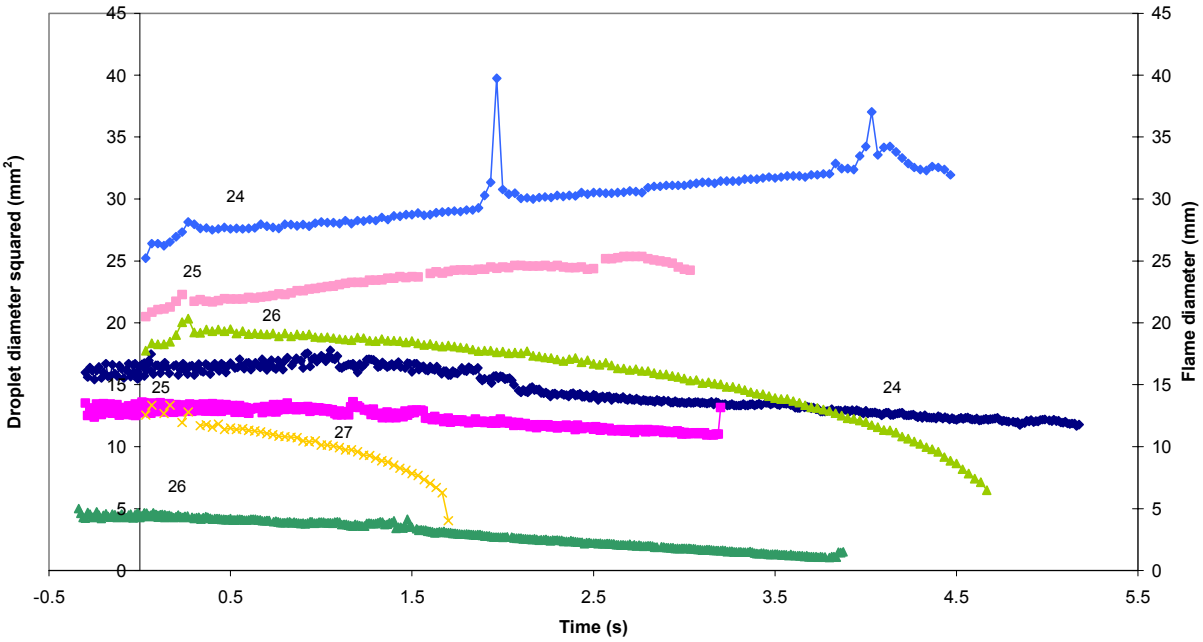

Figure A7: Graphs of droplet diameter squared and flame diameter as a function of time for an oxygen-helium environment at one-half bar and with a 35% mole fraction of oxygen.

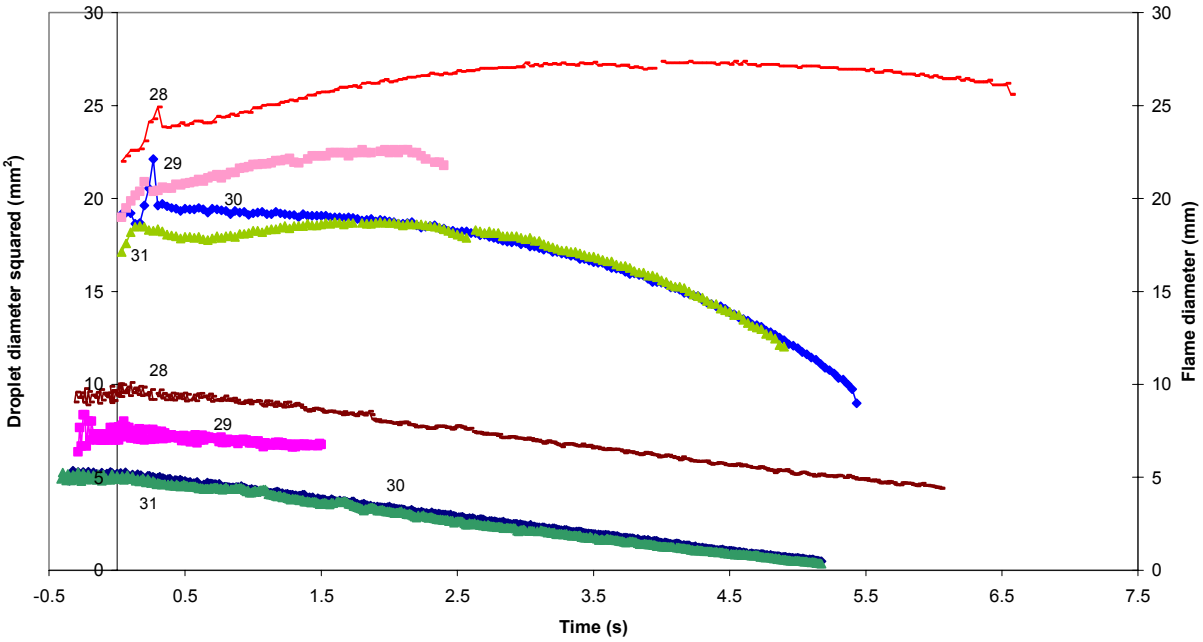

Figure A8: Graphs of droplet diameter squared and flame diameter as a function of time for an oxygen-helium environment at one-half bar and with a 30% mole fraction of oxygen.

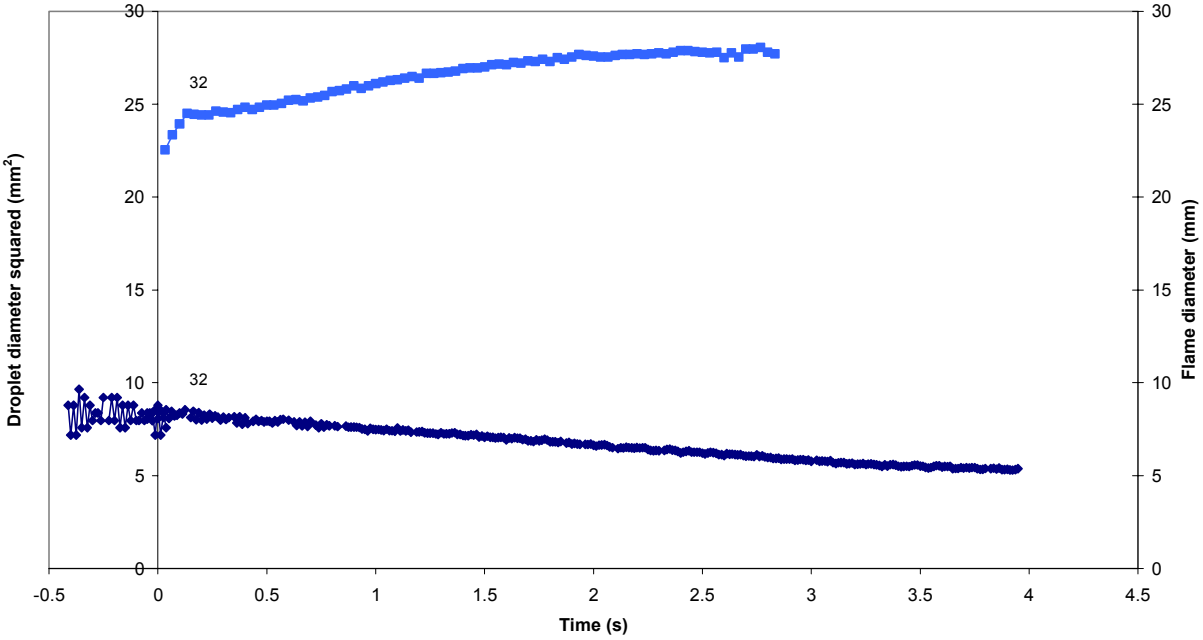

Figure A9: Graphs of droplet diameter squared and flame diameter as a function of time for an oxygen-helium environment at one-half bar and with a 25% mole fraction of oxygen.

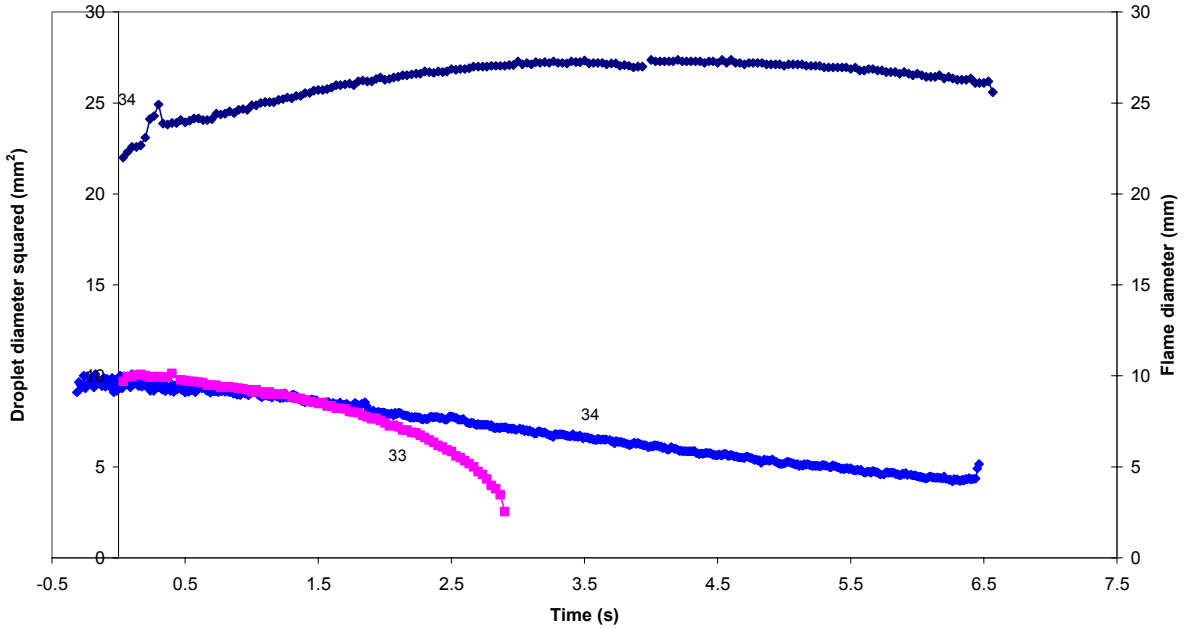

Figure A10: Graphs of droplet diameter squared and flame diameter as a function of time for oxygen-helium environments at one-quarter bar and with 35% or 50% mole fraction of oxygen.

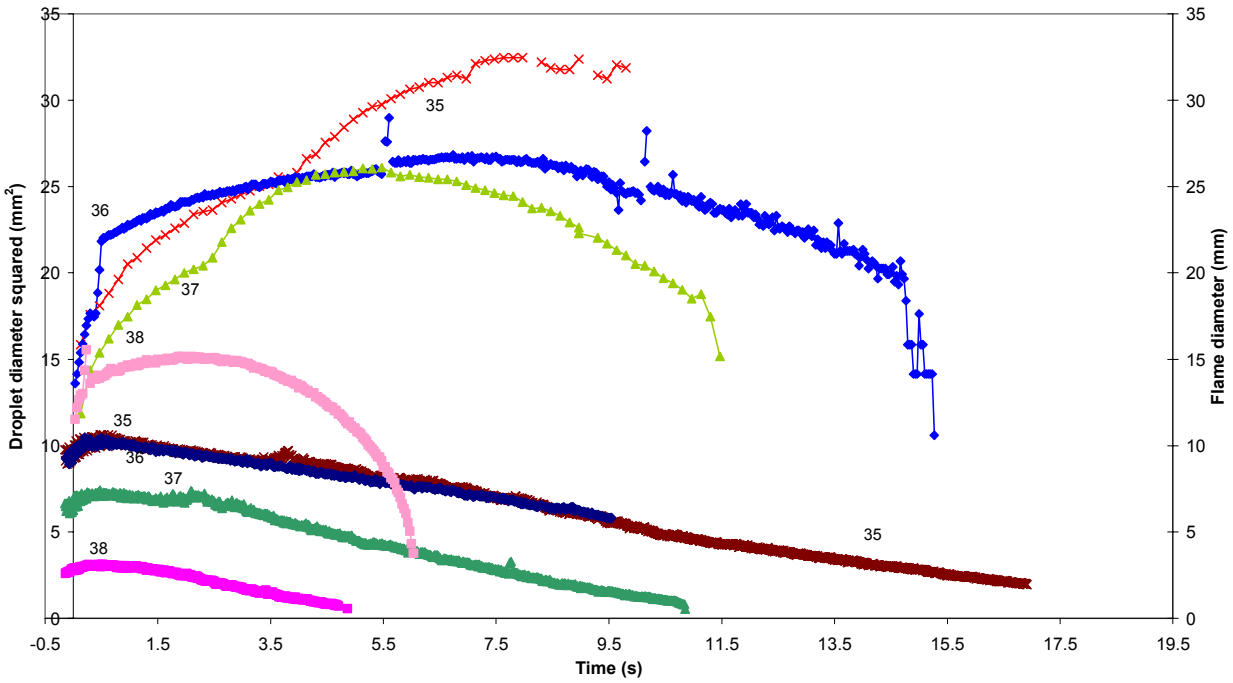

Figure A11: Graphs of droplet diameter squared and flame diameter as a function of time for an environment of Spacelab cabin air at one bar.

Appendix B: FSDC Data

This appendix presents the raw data for the FSDC experiments. The numbering system is the same as in the main text and is summarized in Table 2. The method of data reduction is described in the main text. The final graph in this appendix contains all 15 FSDC tests involving heptane in quiescent air. Graphs for three of the larger droplets end at appreciable droplet diameters because the lighting became too dim to distinguish the edge of the droplet.

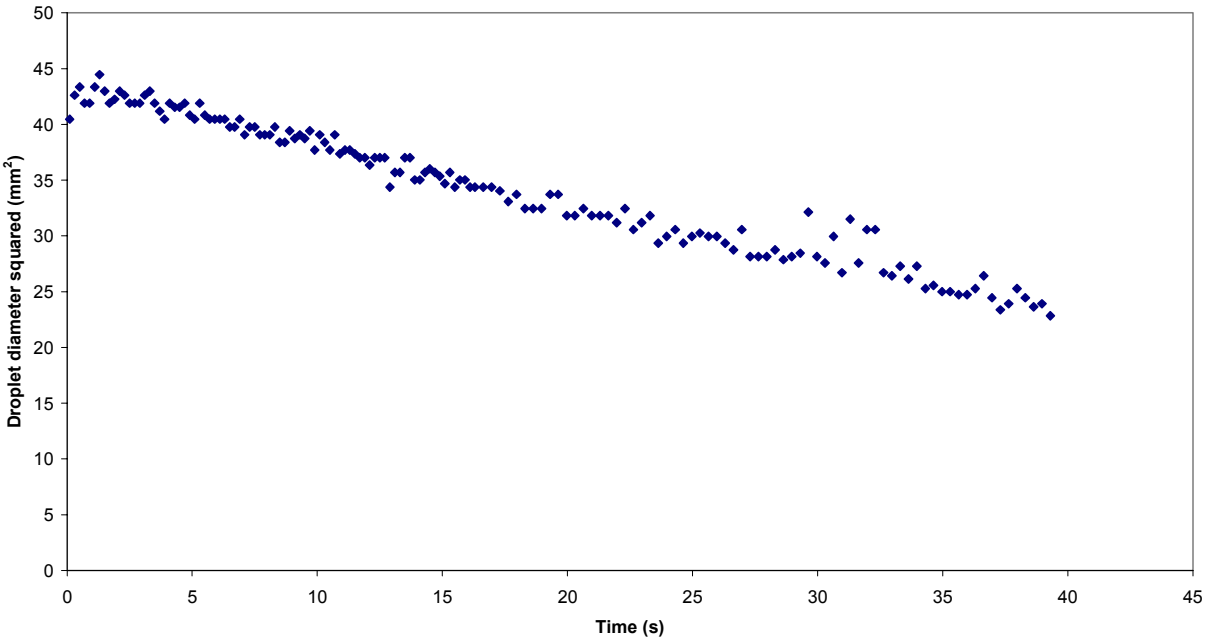

Figure B1: Graph of droplet diameter squared as a function of time for FSDC test 39.

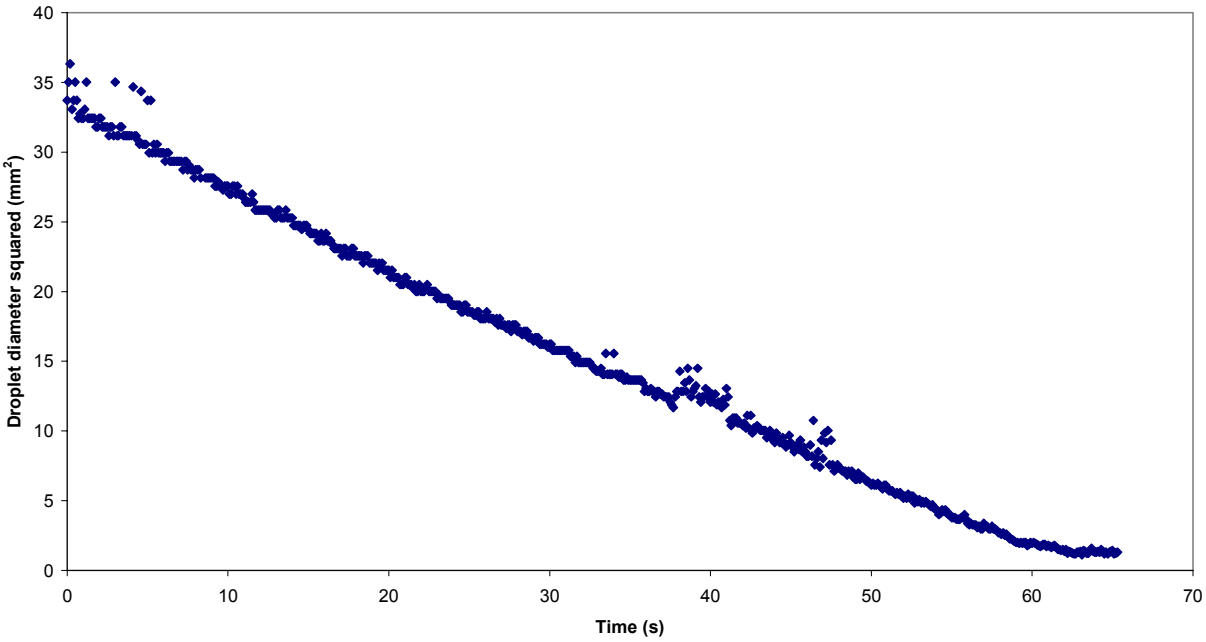

Figure B2: Graph of droplet diameter squared as a function of time for FSDC test 40.

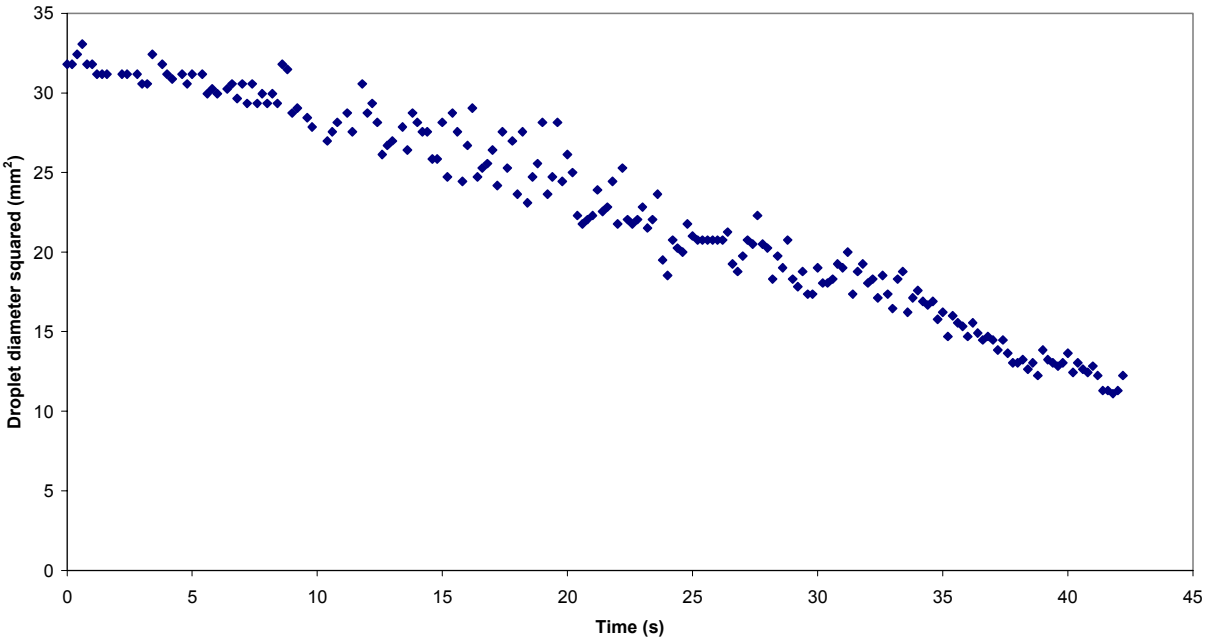

Figure B3: Graph of droplet diameter squared as a function of time for FSDC test 41.

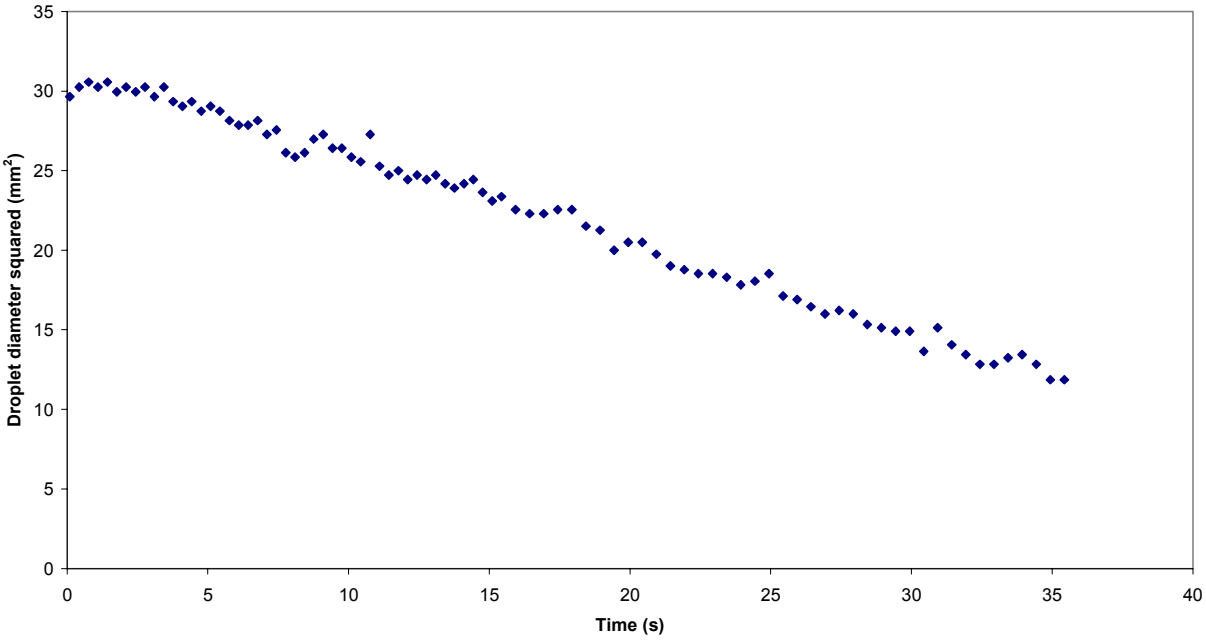

Figure B4: Graph of droplet diameter squared as a function of time for FSDC test 42.

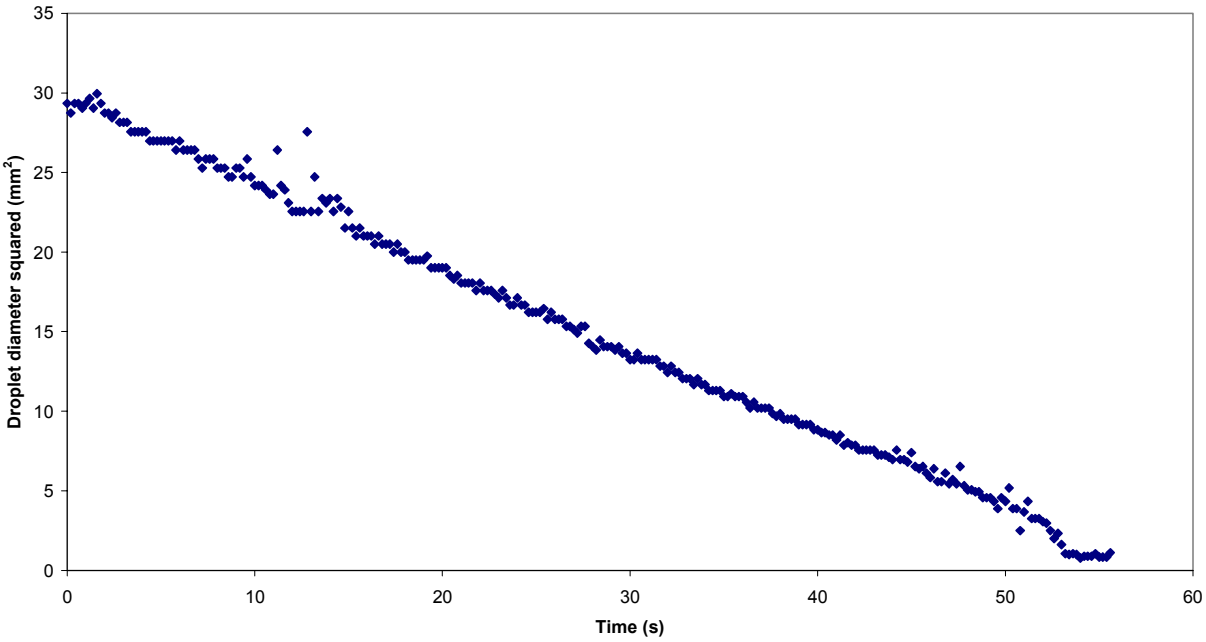

Figure B5: Graph of droplet diameter squared as a function of time for FSDC test 43.

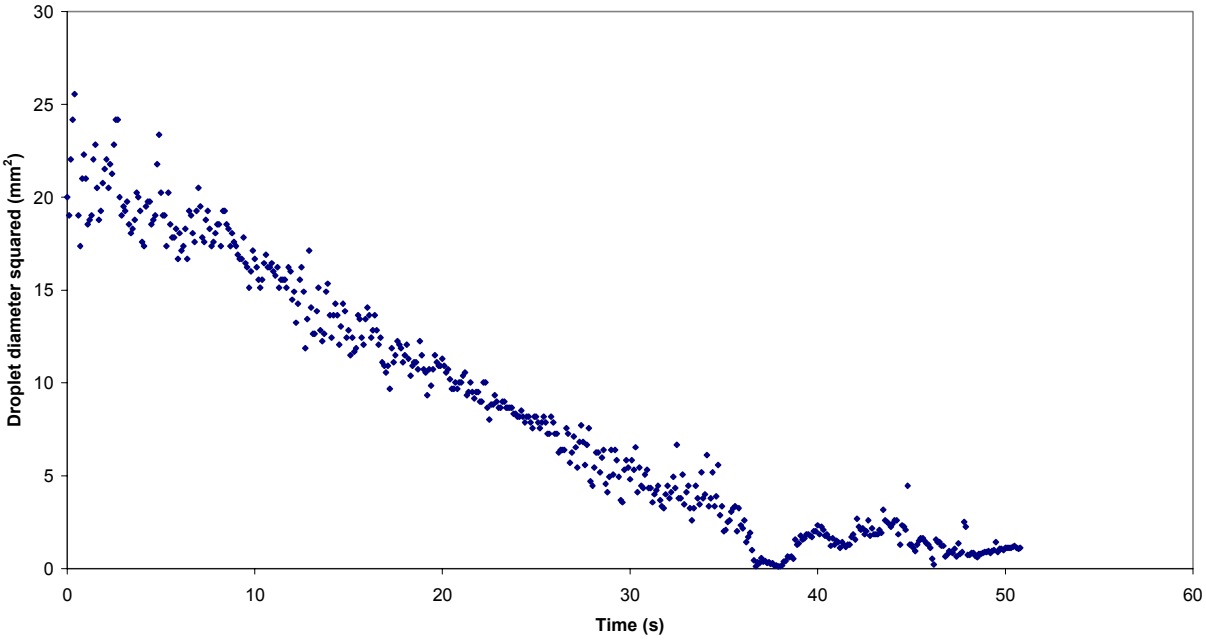

Figure B6: Graph of droplet diameter squared as a function of time for FSDC test 44.

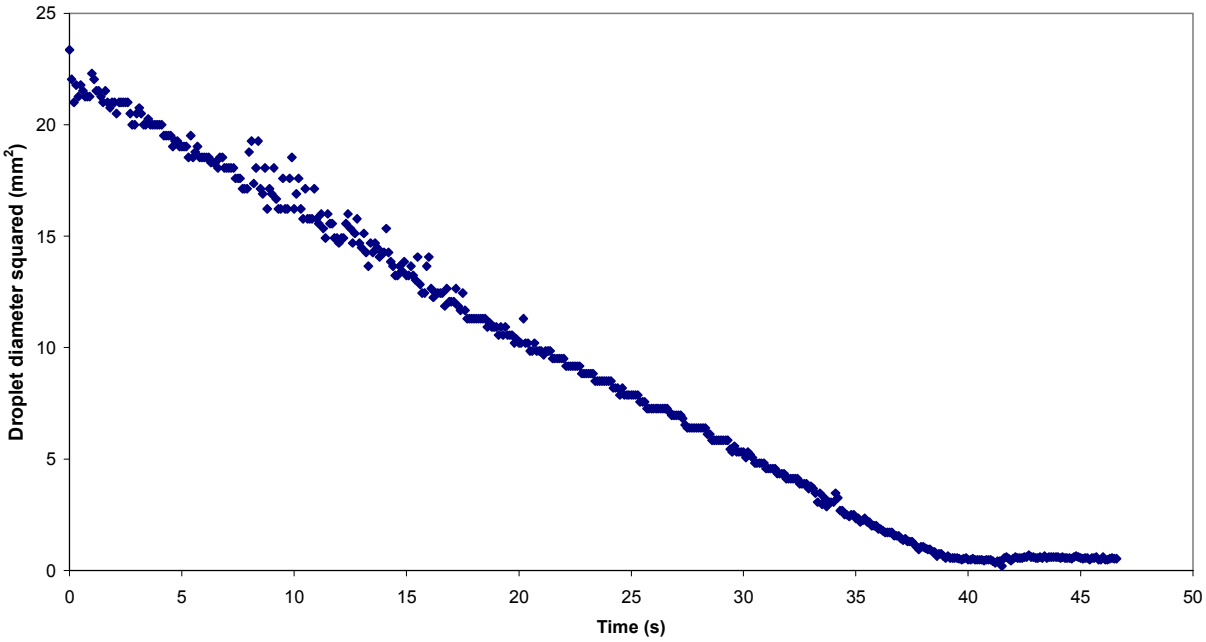

Figure B7: Graph of droplet diameter squared as a function of time for FSDC test 45.

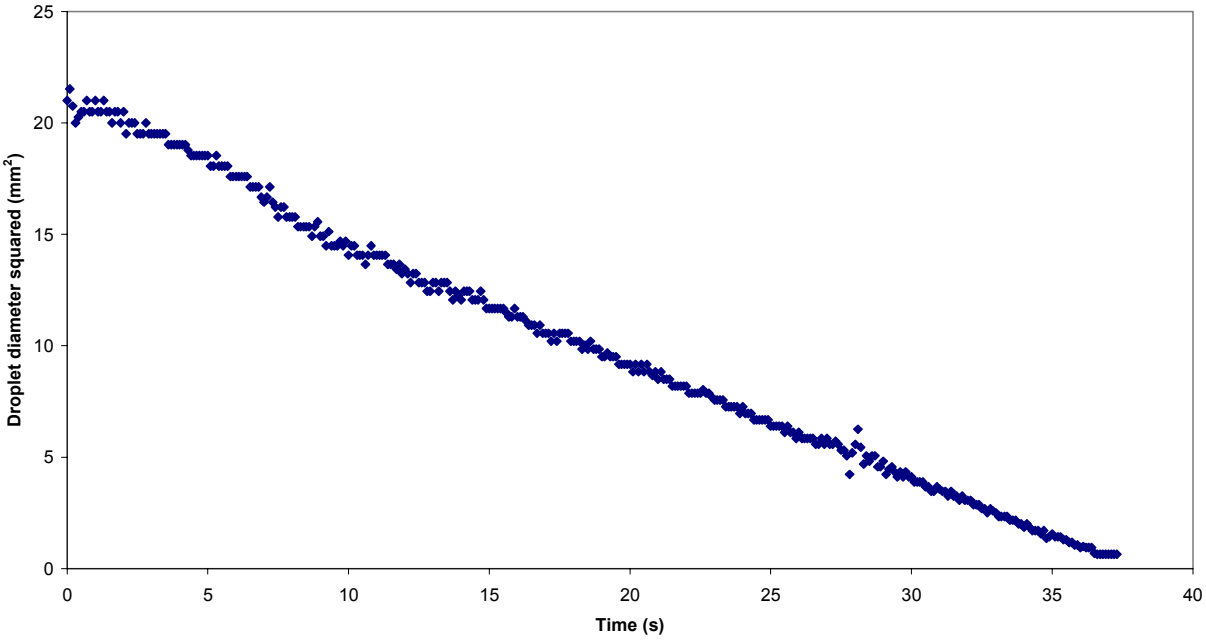

Figure B8: Graph of droplet diameter squared as a function of time for FSDC test 46.

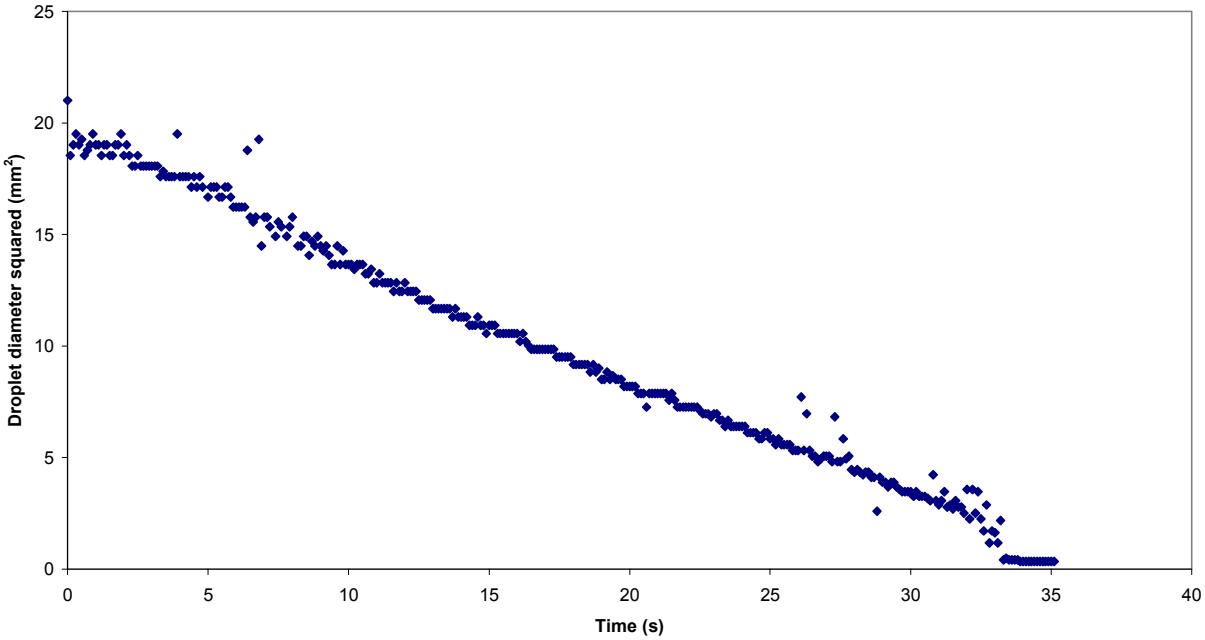

Figure B9: Graph of droplet diameter squared as a function of time for FSDC test 47.

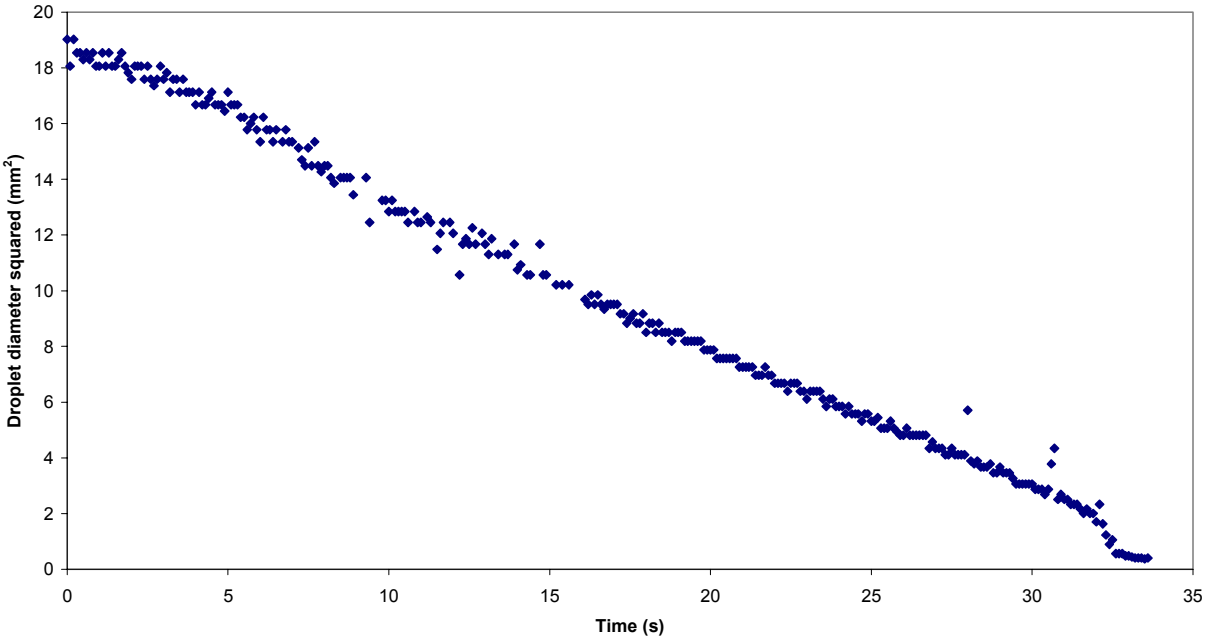

Figure B10: Graph of droplet diameter squared as a function of time for FSDC test 48.

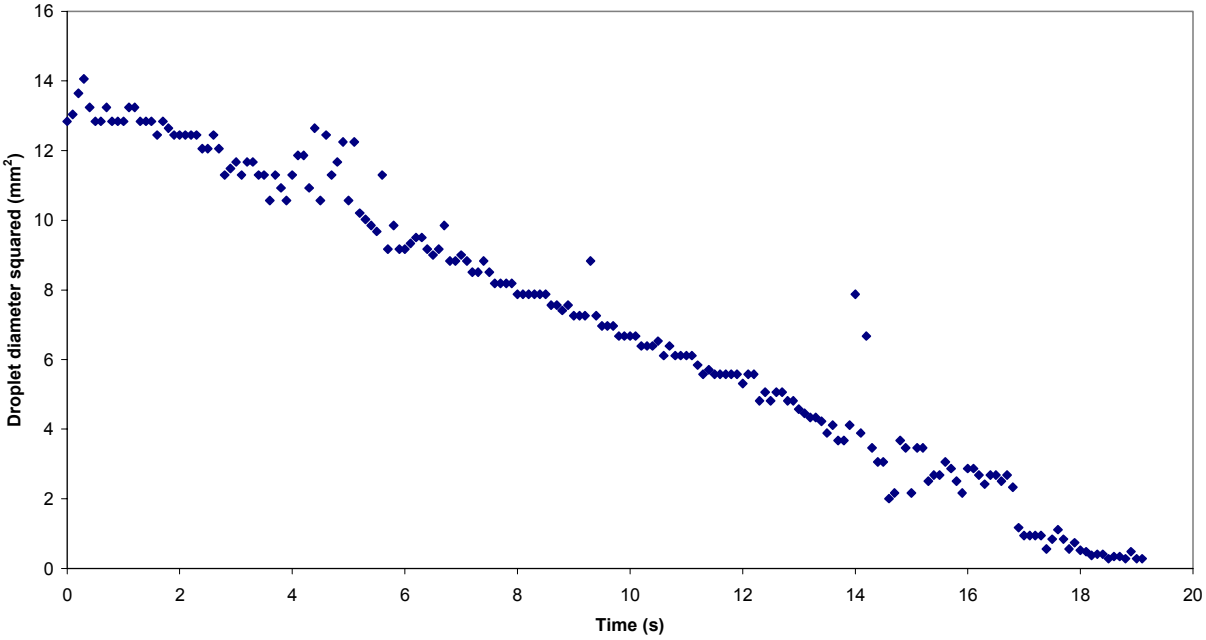

Figure B11: Graph of droplet diameter squared as a function of time for FSDC test 49.

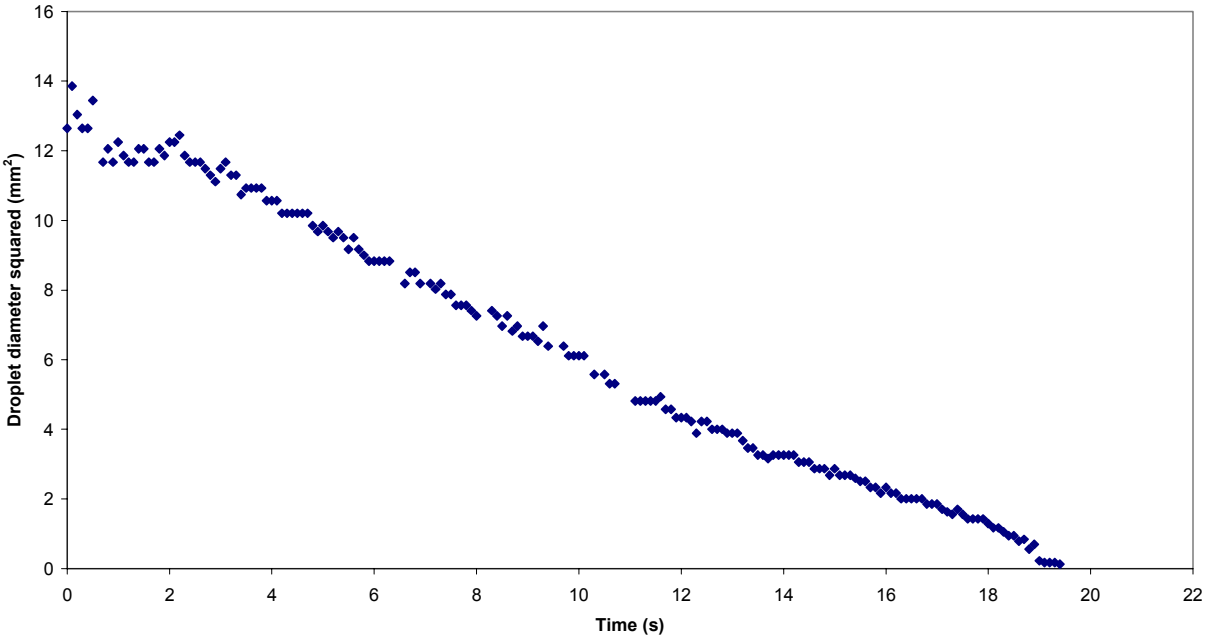

Figure B12: Graph of droplet diameter squared as a function of time for FSDC test 50.

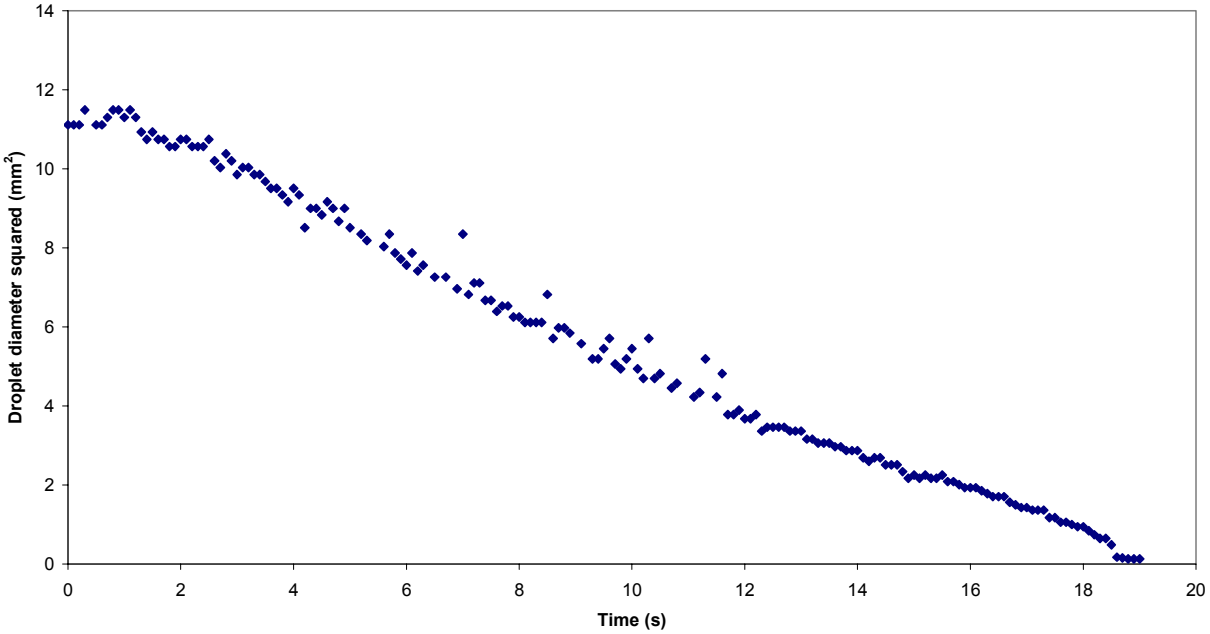

Figure B13: Graph of droplet diameter squared as a function of time for FSDC test 51.

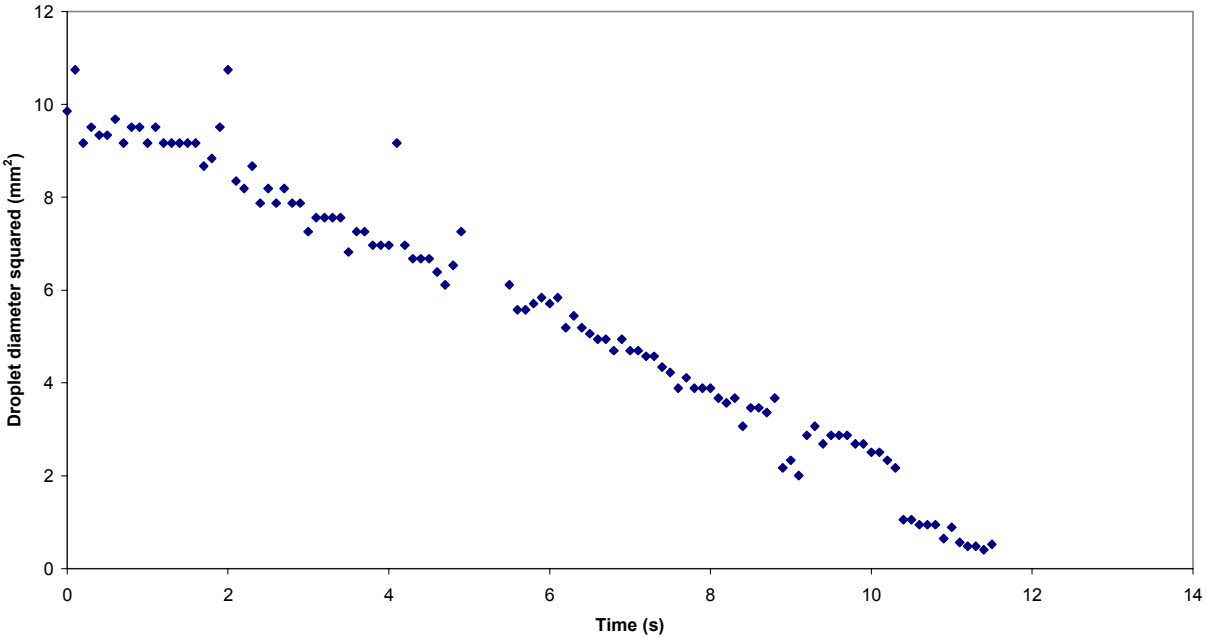

Figure B14: Graph of droplet diameter squared as a function of time for FSDC test 52.

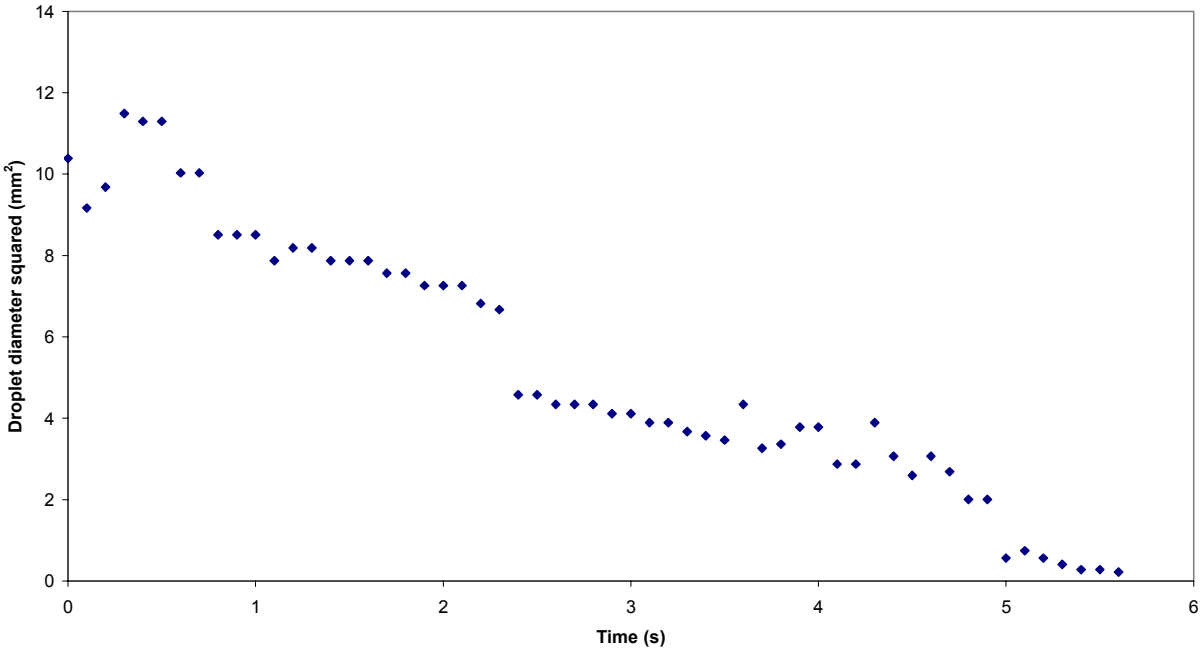

Figure B15: Graph of droplet diameter squared as a function of time for FSDC test 53.

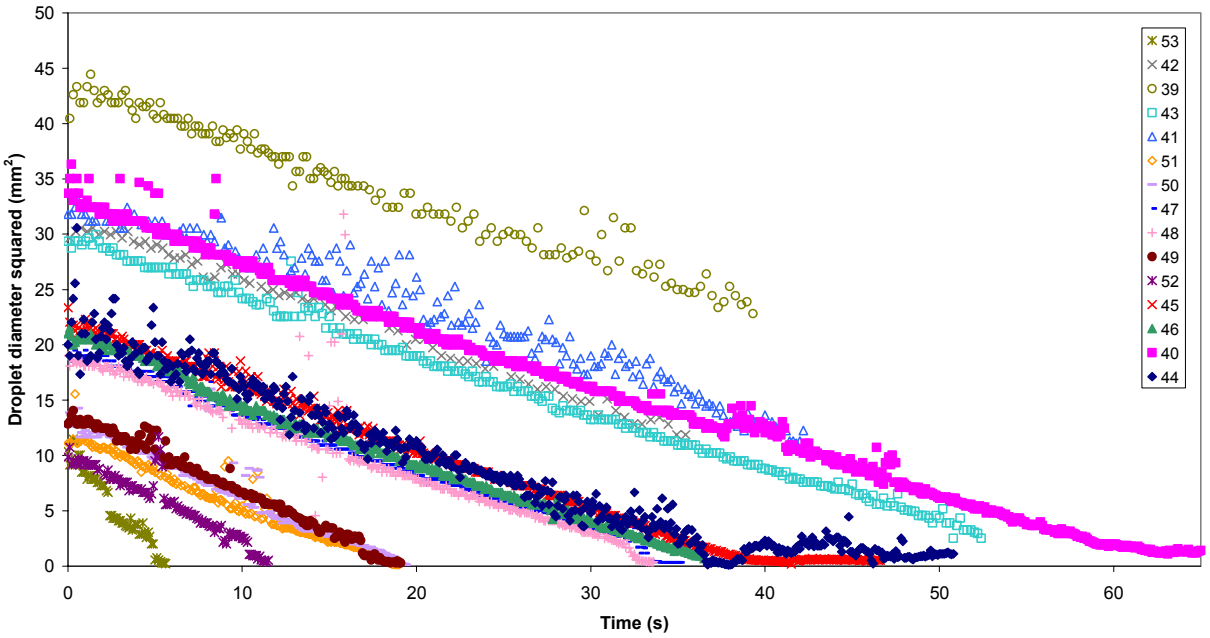

Figure B16: Graph of droplet diameters squared as a function of time for all fifteen FSDC tests analyzed in this paper.

Appendix C: Effects of Fiber Support

Fine fibers supported each droplet to hold it in place during all of the FSDC tests and during two of the four DCE tests in air. Although the combustion is qualitatively the same in many respects with and without the fiber support, there are quantitative influences of the fiber on the results. Quantitative estimates of effects of fiber supports therefore are relevant to interpretation of the data. The purpose of this appendix is to review the effects of the fibers and to provide quantitative estimates.

A droplet on a fiber is not exactly spherical but instead is elongated in the direction of the fiber axis. The extent of this elongation has been measured and taken into account in data reduction,[3] and successful theoretical descriptions have been developed.[9,10] As has been indicated in the text, some bubbling was observed in the liquid for fiber-supported droplets, which is not present for free droplets; influences of the bubbling have been indicated previously and therefore are not discussed here. Possible influences of the fiber on soot behavior, including promotion of migration of soot into the liquid, also have been discussed previously. Finally, where the flame intersects the fiber support, there is a small quench region around the fiber, and heat transfer occurs from the flame across this region and along the fiber by conduction. Quantitative estimates of possible influences of this heat transfer on the burning rate are worthwhile, especially since Fig. 15 shows that burning-rate constants are about 10% larger for fiber-supported DCE droplets than for free DCE droplet and about 20% higher for FSDC droplets. These estimates require information on the thermal and heat-transfer properties of the wires and, for the FSDC experiments, on those of the beads that hold the droplet in position along the wire.

To gauge the effects of heat conduction by the fiber support on the droplet burning rate a comparison was made between the approximate amount of heat conducted along the wire and the approximate amount of heat required for vaporization of the liquid fuel. For both of these calculations an approximate droplet or flame diameter was needed. On the basis of DCE observations, estimates were made mainly for an average case of a droplet diameter of 3 mm and a flame diameter of about 30 mm. In view of the heptane latent heat of vaporization of 76 cal/g and liquid density of 0.7 g/cm^3, the observed burning-rates constants between 0.5 and 0.8 mm^2/s provide a range of required heat-absorption rates for these droplets between about 0.1 and 0.3 W. Estimated rates of heat input to the liquid from fiber supports are to be compared with this total heat-rate requirement.

To calculate the rate of heat conduction along the fiber, the wire diameter and thermal conductivity of the wire must be known. Specifications of the DCE and FSDC wires were given in the FSDC section. They both are about 80 microns in diameter, but their compositions and suppliers differ. The wires are made from the elements carbon, silicon and oxygen in different proportions. Phase diagrams of this three-component system are helpful in ascertaining differences.[11,12] The FSDC wires were of spatially uniform composition with a significant oxygen content, but the DCE wires were constructed by vapor deposition of silicon carbide on a fine carbon filament, with a slightly enriched carbon content deposited at the external surface. The thermal conductivities of materials composed of the three-component system depend not only on the elemental composition but also on the grain structure and types of materials processing and wire construction. Although it might be supposed that variation in thermal conductivities with these parameters would not be large, in fact values can range from about 0.4 to almost 500 W/m K, a variation of more than three orders of magnitude. In addition, changes in conductivities with temperature may be large, exceeding an order of magnitude when temperatures vary from 300 to 1500 K, and the conductivities may increase or decrease with temperature for different materials.

The Nicalon wire of FSDC is reported to have a room-temperature thermal conductivity of 1.4 W/m K, [13] but data are unavailable on its temperature dependence. The Textron fiber used in DCE, on the other hand, is more nearly a pure silicon carbide, whose thermal conductivity is reported[14] to vary from 490 W/m K at 300 K to around 6 W/m K at 2300 K. A five-term fit to the silicon carbide conductivity data[14] was employed to calculate the heat flow rate into the droplet from the flame for the DCE tests, assuming the wire temperature at the flame position to lie between 1000 and 2000 K; values ranging from 2×10^{-2} to 4×10^{-2} W were obtained. The conclusion that can be drawn from these estimates is that heat conduction along the fiber could well provide the 10% increase in burning rate observed for DCE.

If the reported room-temperature thermal conductivity of the Nicalon wire is employed, then the rate of heat conduction to the droplet along the wire is estimated to be only about 3×10^{-4} W for the FSDC tests, which is entirely negligible. To explain the experimentally observed higher burning rate for FSDC on the basis of heat conduction along the wire alone, an average conductivity between 100 and 200 W/m K is needed, twice that of the Textron and about two orders of magnitude greater than the reported room-temperature value. Although, in view of current uncertainties, it is quite possible that the thermal conductance of the Nicalon wire increases rapidly with temperature and is large enough, on the average, to explain the observed FSDC burning-rate increases of about 20%, it is also relevant to seek other possible reasons for the higher burning rates and greater bubbling observed for FSDC. A possible explanation lies in radiative heat transfer to the bead on the FSDC wire. The bead was a porous material with an irregular surface that through multiple reflections could be an efficient absorber of radiant energy and generator of bubble nucleation sites. Radiant energy transfer estimates[15,16] indicate that sufficient energy may be absorbed by the bead to increase the burning rate by perhaps 10%. These estimates, however, are not entirely conclusive, and in view of current uncertainties concerning thermal conductivities, the exact cause of the increased burning rate remains to be determined.

REPORT DOCUMENTATION PAGE

Form Approved
OMB No. 0704-0188

1. AGENCY USE ONLY (*Leave blank*)	2. REPORT DATE	3. REPORT TYPE AND DATES COVERED
	October 2003	Technical Memorandum

4. TITLE AND SUBTITLE

A Treatment of Measurements of Heptane Droplet Combustion Aboard MSL–1

5. FUNDING NUMBERS

WBS–22–101–42–02

6. AUTHOR(S)

M.D. Ackerman, R.O. Colantonio, R.K. Crouch, F.L. Dryer, J.B. Haggard, G.T. Linteris, A.J. Marchese, V. Nayagam, J.E. Voss, F.A. Williams, and B.L. Zhang

7. PERFORMING ORGANIZATION NAME(S) AND ADDRESS(ES)

National Aeronautics and Space Administration
John H. Glenn Research Center at Lewis Field
Cleveland, Ohio 44135–3191

8. PERFORMING ORGANIZATION REPORT NUMBER

E–14119

9. SPONSORING/MONITORING AGENCY NAME(S) AND ADDRESS(ES)

National Aeronautics and Space Administration
Washington, DC 20546–0001

10. SPONSORING/MONITORING AGENCY REPORT NUMBER

NASA TM—2003-212553

11. SUPPLEMENTARY NOTES

M.D. Ackerman, F.A. Williams, and B.L. Zhang, University of California, San Diego, La Jolla, California 92093; R.O. Colantonio and J.B. Haggard, NASA Glenn Research Center; R.K. Crouch, NASA Headquarters; F.L. Dryer and A.J. Marchese, Princeton University, Princeton, New Jersey 08544; G.T. Linteris, National Institute of Standards and Technology, Gaithersburg, Maryland 20899; V. Nayagam, National Center for Microgravity Research; and J.E. Voss, NASA Johnson Space Center. Responsible person, V. Nayagam, organization code 6711, 216–433–8702.

12a. DISTRIBUTION/AVAILABILITY STATEMENT

Unclassified - Unlimited
Subject Category: 29 Distribution: Nonstandard

Available electronically at http://gltrs.grc.nasa.gov

This publication is available from the NASA Center for AeroSpace Information, 301–621–0390.

12b. DISTRIBUTION CODE

13. ABSTRACT ***(Maximum 200 words)***

Results of measurements on the burning of free n-heptane droplets (that is, droplets without fiber supports) performed in Spacelab during the flights of the first Microgravity Science Laboratory (MSL–1) are presented. The droplet combustion occurred in oxidizing atmospheres which were at an ambient temperature within a few degrees of 300 K. A total of 34 droplets were burned in helium-oxygen atmospheres having oxygen mole fractions ranging from 20 to 50 percent, at pressures from 0.25 to 1.00 bar. In addition, 4 droplets were burned in air at 1.00 bar, bringing the total number of droplets for which combustion data were secured to 38; two of these four air tests were fiber-supported to facilitate comparisons with other fiber-support experiments, results of which also are given here. Initial diameters of free droplets ranged from about 1 to 4 mm. The primary data obtained were histories of droplet diameters, recorded in backlight on 35 mm film at 80 frames per second, and histories of flame diameters, inferred from emissions through a narrow-band interference filter centered at the 310 μm OH chemiluminescent ultraviolet band, recorded at 30 frames per second by a intensified-array camera. These data are reported here both in raw form and in a smoothed form with estimated error bars. In addition, summaries are presented of measured burning-rate constants, final droplet diameters, and final flame diameters. Both diffusive and radiative extinctions were exhibited under different conditions. Although some interpretations are reported and conclusions drawn concerning the combustion mechanisms, the principal intent of this report is to provide a complete, documented data set for future analysis.

14. SUBJECT TERMS	15. NUMBER OF PAGES
Microgravity; Combustion; Fires; Flammability; Droplet combustion	49
	16. PRICE CODE

17. SECURITY CLASSIFICATION OF REPORT	18. SECURITY CLASSIFICATION OF THIS PAGE	19. SECURITY CLASSIFICATION OF ABSTRACT	20. LIMITATION OF ABSTRACT
Unclassified	Unclassified	Unclassified	